Tellus (1991), *43AB*, 53–81

Physical initialization for numerical weather prediction over the tropics

By T. N. KRISHNAMURTI, JISHAN XUE, H. S. BEDI, KEVIN INGLES and D. OOSTERHOF,
Department of Meteorology, Florida State University, Tallahassee, Florida 32306 USA

(Manuscript received 18 July 1990; in final form 28 November 1990)

ABSTRACT

The current operational World Weather Watch over the tropical latitudes exhibits large data gaps. This paper proposes a detailed physical initialization procedure where the combined use of the World Weather Watch and detailed satellite data sets are used to enhance the definition of initial surface fluxes of water vapor and sensible heat, the initial rainfall rates and the earth's radiation budget. The satellite radiances are used to unify the physical initializations of the fluxes, rainfall, and the clouds. This is carried out using a Newtonian relaxation during a pre integration phase between day −1 and day 0 where the fluxes, the rainfall rates, and the cloud distributions provide a consistent humidity analysis and a spin up of the diabatic heating and the divergent circulations. A comparison of medium range forecasts from a control experiment (that utilizes the standard nonlinear normal mode initialization, with physics, at day 0) with an experiment based on the unified physical initialization is carried out to demonstrate the effective enhancement of the World Weather Watch over the tropics by the proposed method. These experiments are carried out with a global spectral model which is run at a resolution of 106 wave triangular truncation.

1. Introduction

Difficulties in numerical weather prediction over the low latitudes stem largely from data problems and from the overall treatment of diabatic processes. The current data coverage is described by the elements of the World Weather Watch (WWW, a list of symbols and acronyms is presented in Appendix A). This includes surface based networks of the radiosonde rawinsonde and the pilot balloon distributions, commercial ships and aircraft observations, soundings from the polar orbiting satellites and the cloud-tracked winds from the geostationary satellites. In spite of this diverse asynoptic surface and space based system, large data gaps are evident over both the land and the oceanic areas of the tropics. The initialization of surface fluxes of moisture and sensible heat, precipitation and clouds is contaminated by the sparsity of data. The distribution of humidity is very important in this regard. The analysis of the humidity variables relies only on the available radiosonde network. Fig. 1 shows a typical tropical distribution of the "RAOB" network. This illustration is taken from the files of ECMWF, it shows the RAOB network during 1–15 January 1984 at 00 UTC. The obvious data gaps are not simply remedied by a first guess provided by the forecasts of a data assimilation system. Unlike in the extratropics, where the quasigeostrophic vertical motions usually carve out a reasonable moisture field, the locale of the tropical deep convection are poorly described when one starts out with large errors in the humidity distributions. The sparsity of data also results in large errors in the divergent wind which in turn usually compounds the humidity errors through moisture convergence, resulting in erroneous specification of the diabatic forcing. An inherent spin up problem exists in most global prediction models. The nature of the spin up reveals itself in a slow equilibration of the global evaporation and precipitation over a period of some 3 to 4 days. During this period the divergent motion, the diabatic heating and the surface pressure field undergo an adjustment. The spin up arises from inconsistencies of the

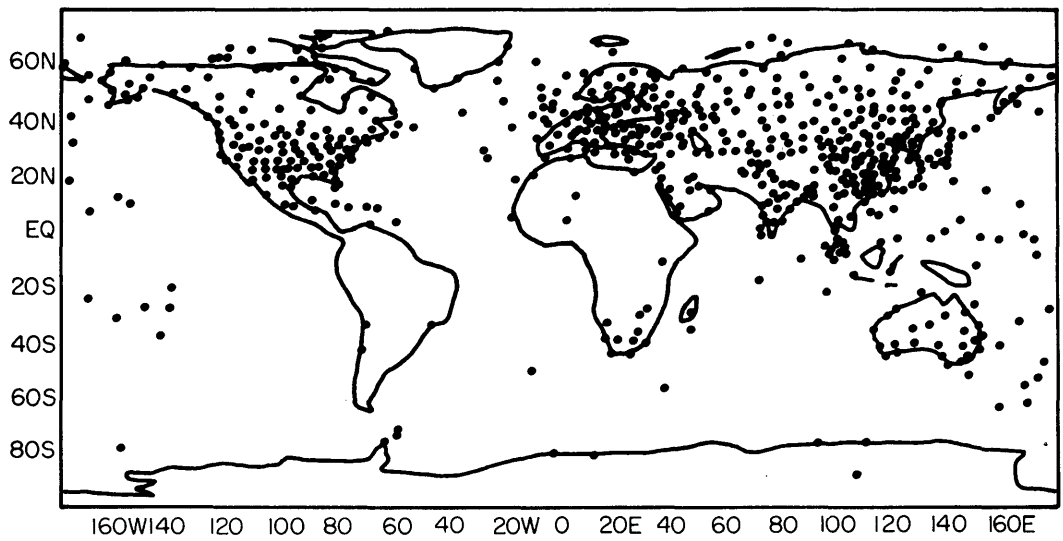

Fig. 1. The distribution of upper air network of stations reporting data during 1–15 January 1984. Map based on operational ECMWF archives. The data gaps over the tropics and southern hemisphere are most conspicuous.

initial fields with the dynamics and physical parameterizations of the model. A too dry lower troposphere can lead to an enhancement of the evaporation from the ocean and also to a reduction of the rainfall rates. This results in a slow equilibration of the humidity field, especially in the tropics; and manifests in the overall spin-up, as was also noted by Heckley (1985). Such initial deficiencies in the humidity analysis are not addressed by the normal "dynamical" type initialization procedures such as NLNMI. There is thus a need for addressing all of the moist processes to which the moisture analysis is sensitive. Future satellite systems under the Earth Observing System (EOS) program hold promise from the Laser Atmospheric Wind System (LAWS), the microwave technology of Tropical Rainfall Measurement Mission (TRMM) and the Atmospheric Infrared Radiation Sounder (AIRS). These are expected to provide high resolution measures of winds, rainfall rates, moisture, temperature and humidity and thus improve the current network. That is expected to happen in the late 1990s.

At the present time, some improvement in the definition of the initial state of the tropical atmosphere is however possible from a mix of the currently available surface and space based observations. The premise here is that the rotational part of the wind, the temperature field, and the surface pressure field can be represented, somewhat reasonably, by the current 4-D assimilation techniques with the currently available observations. The analysis of the humidity variable, rainfall rates, and the divergent wind leave much to be desired. This study incorporates a Newtonian relaxation procedure, in its initialization and makes use of information obtained from the current satellites and from the current World Weather Watch to address this problem.

The initialization procedure consists of two steps. (1) Diagnostic calculations of surface fluxes, humidity analysis consistent with the surface fluxes and observed rainfall rates, humidity analysis consistent with the net outgoing long wave radiation. (2) To incorporate the above (i.e., fluxes, rainfall and clouds) during a preintegration phase, i.e., from day -1 to day 0, via a relaxation process, where in an additional term is added to the model's dynamical and thermodynamical equations. The additional term defines a Newtonian nudging which is aimed to relax the model forecast values

to certain observed estimates. Basically, the procedure is as follows: First we make use of an integral technique, following Yanai et al. (1973), using as input the "observed" rainfall rates and vertically integrated radiative heating rates to obtain diagnostic measures of the surface fluxes of water vapor and sensible heat. This technique provides reasonable estimates of evaporation rates over regions of rainfall over both land and oceanic areas. The use of a reverse similarity theory is next made to generate data sets of these variables on top of the constant flux layer consistent with the prescribed "Fluxes". The next step in this exercise is to deploy a reverse cumulus parameterization algorithm which provides an analysis of the humidity variable above the constant flux layer consistent with the imposed precipitation rates following Krishnamurti et al. (1984, 1988c). A third step in this exercise is an attempt to improve the cloud cover distributions from a matching of the earth's radiation budget as inferred from the radiation algorithm and as measured by the satellites. This results in an improvement of the humidity analysis above the 500 mb surface where the observations of the humidity variable are generally least reliable. A single parameter in a vertical structure function of the humidity variable above 500 mb is determined from a minimization of the difference between the model and the satellite based measures of the outgoing longwave radiation. This entire sequence of steps produces in a diagnostic sense, a thermodynamic consistency between the humidity variable, the surface fluxes, rainfall distributions and the clouds.

This procedure alone, however is, not adequate to provide a diabatic initialization. That is accomplished by a Newtonian relaxation of the above diagnosed humidity variable where the divergent wind is permitted now to evolve in response to the imposed surface fluxes and the condensation heating in a consistent manner. The Newtonian nudging addresses all of the basic variables of the model following a procedure outlined in Krishnamurti et al. (1988c). This Newtonian relaxation is carried out during a preintegration phase prior to day 0 of a medium range prediction experiment. This technique allows the assimilation of the above data, which is additional information to that given by the data distributions shown in Fig. 1.

In this paper we shall describe the elements of this initialization procedure and illustrate its impact in a medium range prediction experiment using a high resolution global spectral model.

2. Yanai fluxes

The surface fluxes of sensible heat (F_S) and moisture (F_L), following Yanai et al. (1973) may be expressed by the relations,

$$F_S\uparrow = \hat{Q}_1 - \hat{Q}_R - LP. \tag{2.1}$$

Here $\hat{Q}_1$ denotes the vertically integrated apparent heat source, where

$$Q_1 = \frac{\partial \bar{s}}{\partial t} + \nabla_\sigma \cdot \overline{sv} + \frac{\partial}{\partial \sigma}\bar{s}\bar{\dot{\sigma}}, \tag{2.2}$$

where $\bar{s}$ is the large scale dry static energy and $\hat{Q}_R$ denotes the vertically integrated net radiative heating;

$$F_L\uparrow = LP - \hat{Q}_2. \tag{2.3}$$

Here, $\hat{Q}_2$ is the vertically integrated apparent moisture sink and P is a measure of the observed rainfall rate.

Where

$$Q_2 = -L\left(\frac{\partial \bar{q}}{\partial t} + \nabla_\sigma \cdot \overline{qv} + \frac{\partial}{\partial \sigma}\bar{q}\dot{\sigma}\right). \tag{2.4}$$

This is basically a moisture balance relation, and in general, over the rain areas, the vertically integrated apparent moisture sink is a small difference between the surface flux of moisture and the precipitation. In the rain free areas, $\hat{Q}_2$ is generally small and matches the surface flux of humidity. The calculation of the fluxes from the surface similarity theory are very sensitive to the extrapolation of the basic variables to the top of the constant flux layer. The vertical integral appraoch of Yanai fluxes provides most of the information for $\hat{Q}_2$ from the deep troposphere and is not sensitive to whatever may be assigned via extrapolation at the top of the constant flux layer.

Figs. 2 and 3 illustrate some sample diagnostic calculations of $\hat{Q}_1$ and $\hat{Q}_2$ during two contrasting periods in the evolution of the monsoon. Fig. 2 corresponds to a dry period prior to the onset of monsoon during 1979. Here the vertically

integrated apparent heat source $\hat{Q}_1$ and the apparent moisture sink $\hat{Q}_2$ are illustrated. Fig. 3 shows the corresponding distribution of $\hat{Q}_1$ and $\hat{Q}_2$ during a wet period subsequent to the onset of the monsoon. These illustrations are based on Huibang and Yanai (1984). Related studies on heat sources from FGGE data sets were performed by Johnson et al. (1987), Kasahara et al. (1987) and several others. The large contrast in the vertically integrated apparent heat sources and moisture sinks appear to be reasonably described by this approach. This is a starting point in our analysis of the surface fluxes.

The FSU global spectral model is described in Appendix 2. This is an X-Y-σ model, it utilizes a horizontal resolution of T106 waves and 12 vertical levels. The model includes a comprehensive array of physical processes. The diagnostic calculations of $\hat{Q}_2$ are carried out in the model coordinates using the spectral transform method for the nonlinear advective terms ($-V \cdot \nabla q$). The vertical advection terms $\dot{\sigma}(\partial q/\partial \sigma)$ is calculated consistent with the vertical finite differencing of the model i.e., an energy conserving scheme. The calculation of Q_2 is time centered between two map times which are 24 h apart. The vertical

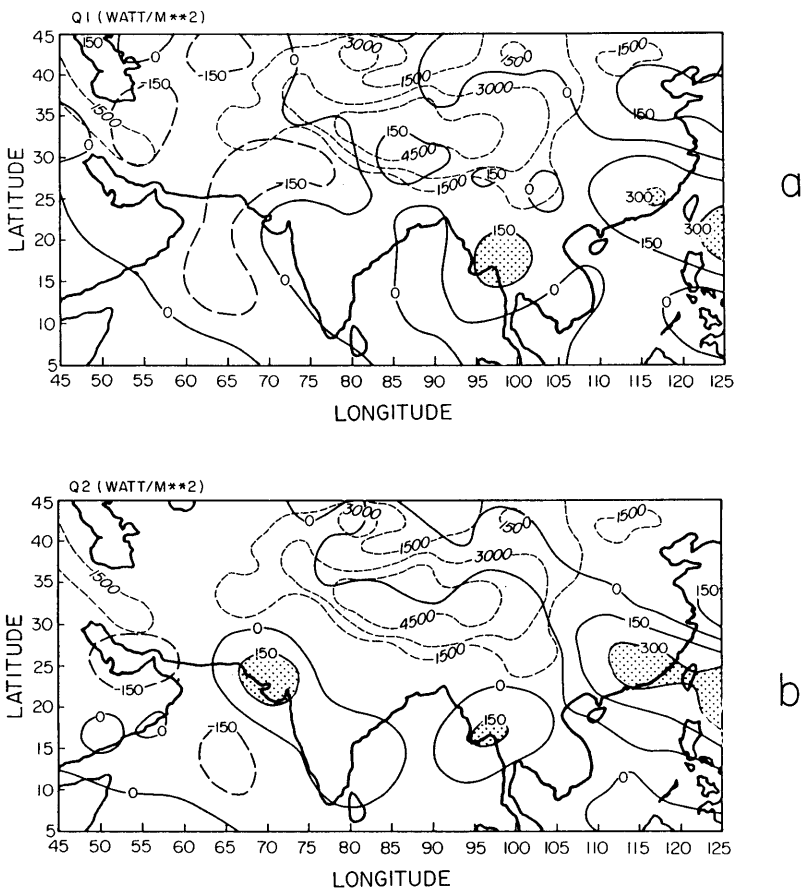

Fig. 2. (a) Distribution of vertically integrated apparent heat source during a pre-monsoon onset phase in 1979. Units: W/m^2, interval 150 W/m^2, Huibang and Yanai (1984). (b) Distribution of vertically integrated apparent moisture sink during a pre-monsoon onset phase in 1979. Units: W/m^2, interval 150 W/m^2, Huibang and Yanai (1984).

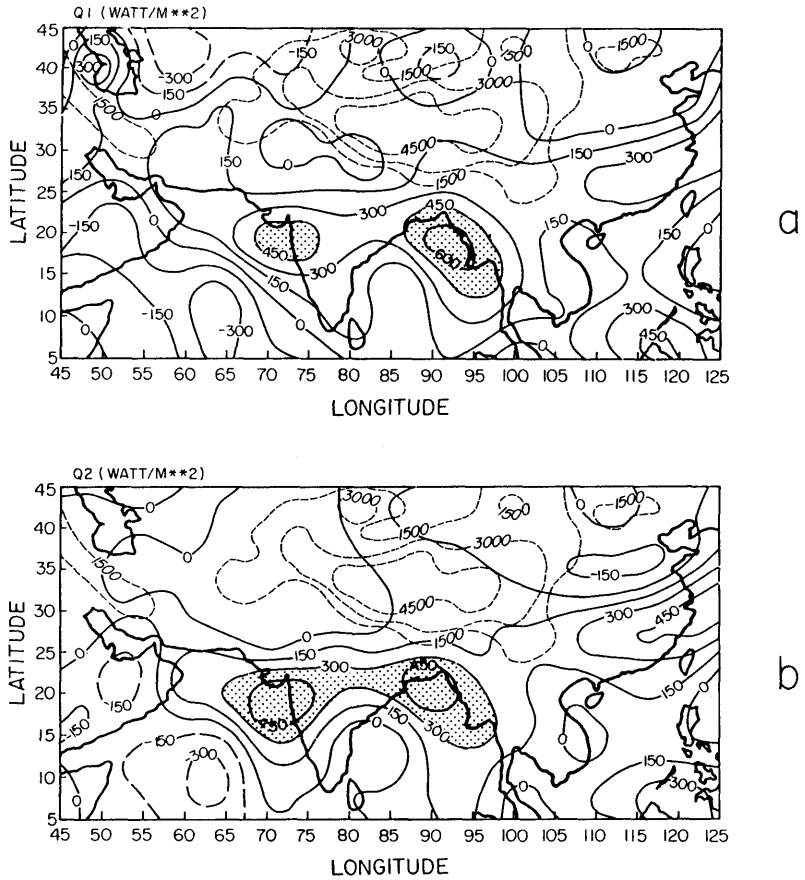

Fig. 3. (a) Same as Fig. 2a but for a post-monsoon onset phase. (b) Same as Fig. 2b but for a post-monsoon onset phase.

integrals cover the range $\sigma = 0$ to $\sigma = 1$. The calculation of $\dot{\sigma}$ requires the usual corrections for the Dines Compensation. $\dot{\sigma}$ is calculated using the following form of the mass continuity equation,

$$\dot{\sigma} = \int_{\sigma=0}^{\sigma} [(\hat{V} - V) \cdot \nabla \ln(p_s) + (\nabla \cdot \hat{V} - \nabla \cdot V)] \, d\sigma. \tag{2.5}$$

The values of $\dot{\sigma}$ thus obtained are automatically corrected for the Dines Compensation following Krishnamurti (1986). The field of $\hat{Q}_2$ is calculated over the entire globe from 24 h of globally analyzed data sets (i.e., 4 data sets per day 6 h apart).

3. Precipitation estimates

We use a mix of raingauge and OLR based regression methods to obtain a field of tropical rainfall. This method is described in a rainfall atlas, Krishnamurti, et al. (1983a). The analysis procedure consists of several steps.

(i) The satellite based OLR data and its local time rate of change are both colocated on to a one degree latitude/longitude grid where averaged raingauge data are prepared. The rainfall rates are regressed against OLR and its time rate of change using three months of data sets. This exercise was carried out with the FGGE IIC raingauge data sets.

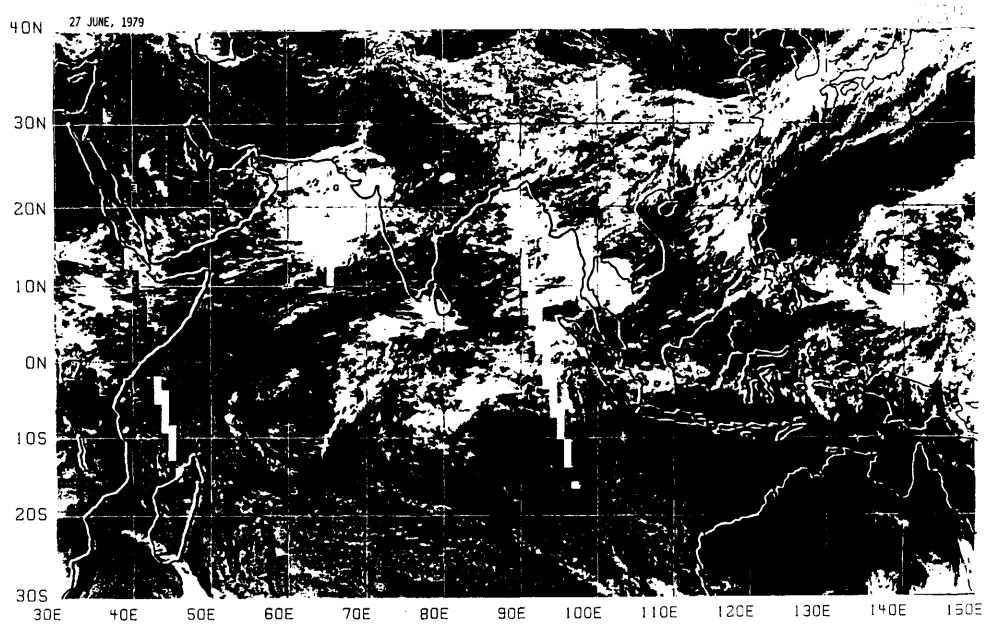

a

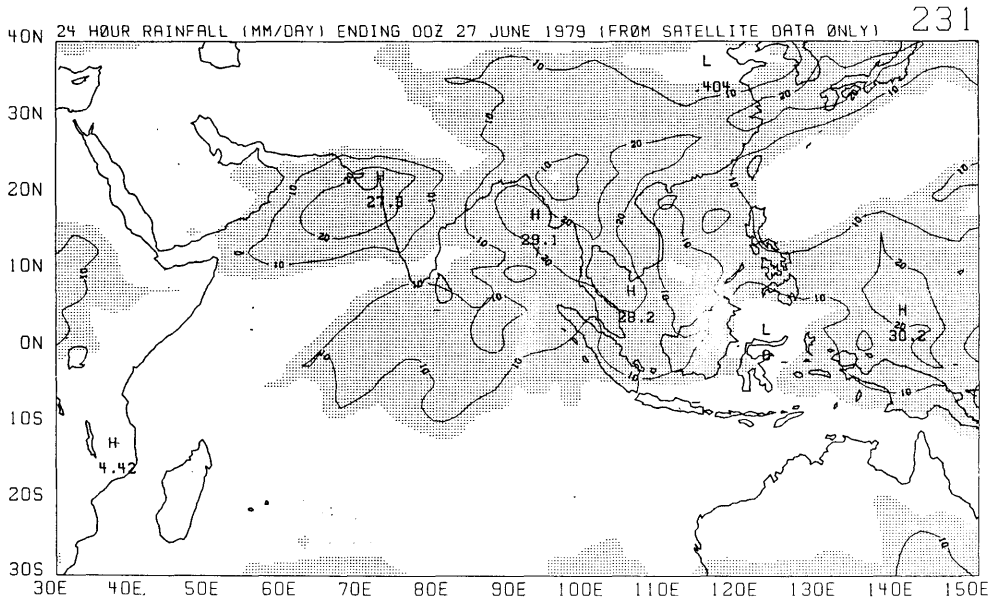

b

Fig. 4. (a) Infrared photograph for 27 June 1979 for the sun synchronous DMSP polar orbiting satellite over the monsoon region. (b) First guess of rainfall derived from outgoing longwave radiation using a regression method. 24-h total in mm/day ending on 27 June 1979 00 UTC. (Shaded area indicates rainfall greater than 7 mm/day.)

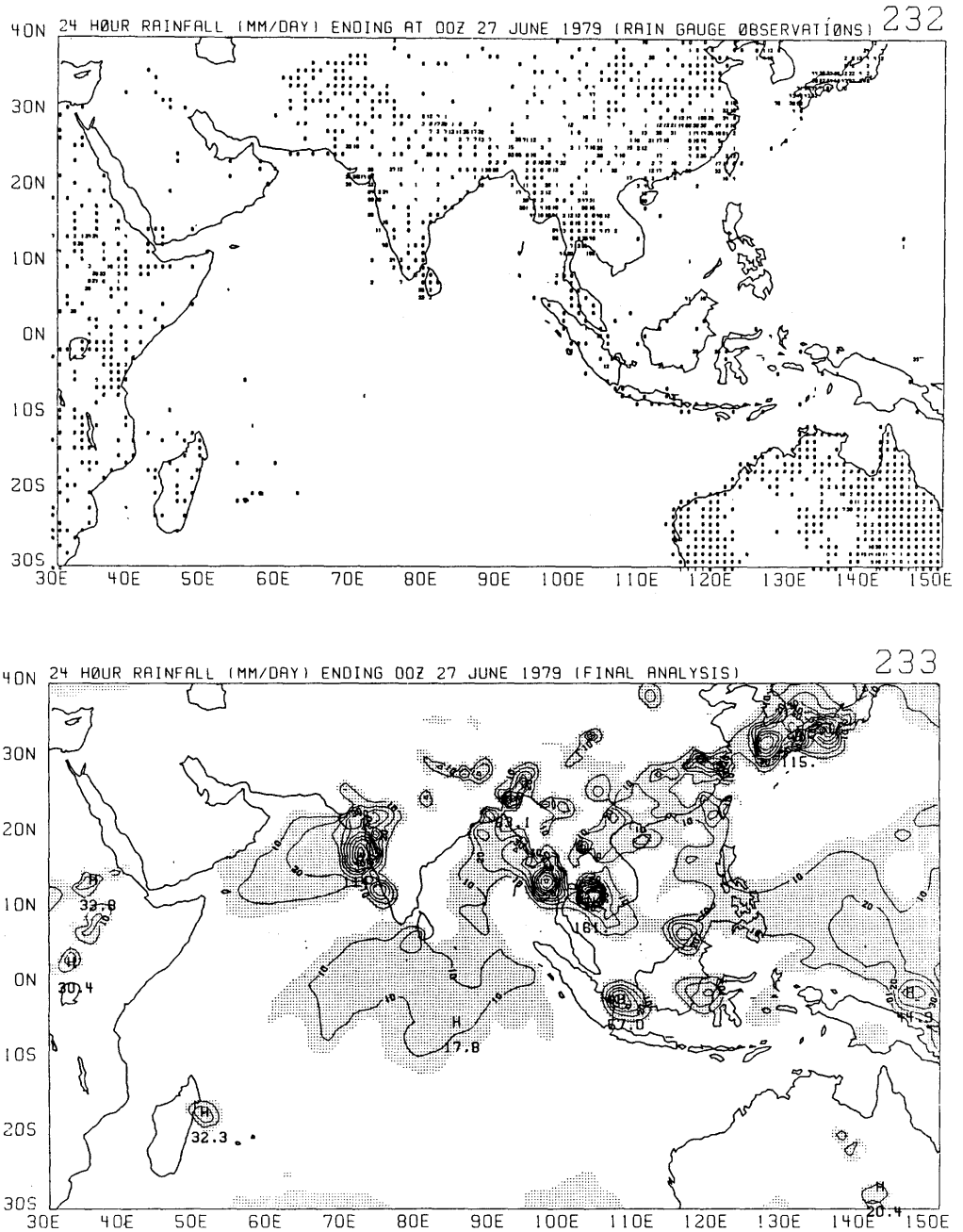

Fig. 4. (c) Raingage data (mm/day) averages as 1° square and 24-h totals ending on 27 June 1979 00 UTC. (d) Estimated final rainfall covering the same 24-h period as in (b) and (c) (mm/day). This makes use of regression plus the raingage data sets.

(ii) The linear regression coefficients, thus obtained, are used to map a first guess daily rainfall field using the daily values of OLR and its time rate of change.

(iii) The next step consists of an objective analysis where some 7,000 raingauge observations per day were analyzed with the above first guess over a global tropical belt between 35° S and 35° N.

This scheme was based on polar orbitor OLR data sets since the global radiance data from five geostationary satellites were not available. This method was found to provide an excellent analysis of daily rainfall rates over the land areas where the raingauge data has a strong influence. Over the oceanic tropics, this method relies largely on the regression, and appears to underestimate the rainfall rates by about a factor of two. A histogram method proposed by Arkin (1979) appears to be more promising over the oceans, however, its use is mostly recommended for time scales larger than a week. Future microwave satellite missions, EOS/TRMM, are expected to provide better temporal coverage.

Fig. 4 illustrates a sample from the regression, objective analysis method used in the present study. The panel (a) shows a satellite photograph over the monsoon region, this illustrates major convective areas during an active monsoon spell. Panel (b) shows the first guess rainfall distribution based on the regression method. Panels (a) and (b) show a very close correspondence, i.e., precipitation is estimated over the cloudy areas. Panel (c) shows the distribution of raingage data averaged over one degree squares. The final analysis of the precipitation rates, shown in panel (d), incorporates the radiance and the raingage data sets. A comparison of panels b and d shows that the objective analysis adds a considerable amount of detail to the first guess field, although away from land areas the final analysis is still largely determined by the first guess field. In spite of the obvious limitations of this approach over the oceanic tropics, we feel that a physical initialization to enhance the model rainfall, surface fluxes and the resulting spin up of divergence from this product appears to be the best one can do with the use of the infrared radiation data from polar orbiting satellites. The use of microwave data such as the SMMI can enhance the resolution and accuracy of the present method. Several research groups are currently exploring the use of the SMMI data sets for the determination of water vapor profile and precipitation rates. This holds promise for the next decade prior to the launch of the EOS platforms.

4. Reverse similarity theory

Given the Yanai fluxes of sensible and latent heat as an input to the similarity theory, one can in principle solve for the potential temperature and the moisture variable on top of the constant flux layer. In the conventional problem, one solves the similarity equations for the variables L, U^*, θ^*, q^*. Here L is the Monin-Obukhov length, the remaining of these variables provide respectively, the momentum, heat and moisture fluxes. Different sets of similarity equations describe the stable ($L>0$) and the unstable ($L<0$) surface layers. In this problem (Businger et al., 1971), the basic variables such as wind, temperature, and moisture at the bottom and top of the constant flux layer and the surface roughness are prescribed. We shall not discuss these equations in detail here since they are provided in standard text books, e.g., Haltiner and Williams (1979), Stull (1988), and in Businger et al. (1971) and in our applications (Chang, 1978 and Krishnamurti et al., 1988a).

We shall, following Chang (1978), express the similarity fluxes of momentum, heat and moisture respectively by the relations

$$F_M = \rho C_M (U_2 - U_1)^2, \tag{4.1}$$

$$F_H = \rho C_p C_H (U_2 - U_1)(\theta_2 - \theta_1), \tag{4.2}$$

$$F_Q = \rho C_q (U_2 - U_1)(q_2 - q_1)\, g_w, \tag{4.3}$$

where the similarity exchange coefficients are expressed as follows.

(a) *For the Stable and neutral case*: $\mathrm{Ri_B} > 0$

$$C_M = \frac{U_*^2}{(U_2 - U_1)^2} = \frac{k^2}{[\ln(Z_2/Z_1)]^2} \frac{1}{(1 + 4.7\,\mathrm{Ri_B})^2}, \tag{4.4}$$

$$C_H = \frac{U_* \theta_*}{(U_2 - U_1)(\theta_2 - \theta_1)} = \frac{-1}{0.74} \frac{k^2}{[\ln(Z_2/Z_1)]^2} \frac{1}{(1 + 4.7\,\mathrm{Ri_B})^2}, \tag{4.5}$$

$$C_q = 1.7 C_H. \tag{4.6}$$

(b) *For the Unstable case*: $\mathrm{Ri_B} < 0$

$$C_M = \frac{U_*^2}{(U_1 - U_2)^2} = \frac{k^2}{[\ln(Z_2/Z_1)]^2}\left(1 - \frac{9.4\,\mathrm{Ri_B}}{1 + C\,|\mathrm{Ri_B}|^{1/2}}\right), \quad (4.7)$$

$$C_H = \frac{U_*\theta_*}{(U_2 - U_1)(\theta_2 - \theta_1)} = \frac{-1}{0.74}\frac{k^2}{[\ln(Z_2/Z_1)]^2} \times \left(1 - \frac{9.4\,\mathrm{Ri_B}}{1 + C\,|\mathrm{Ri_B}|^{1/2}}\right), \quad (4.8)$$

$$C_q = 1.7 C_H. \quad (4.9)$$

Here, Z_1 and Z_2 denote, respectively, the heights of the bottom and top of the constant flux layer. Z_1 is identified with a roughness length Z_0. (U_1, U_2), (θ_1, θ_2) denote the wind and the potential temperature at the bottom and top of the surface layer. $\mathrm{Ri_B}$ denotes the Bulk Richardson number whose sign is used here to determine the stability, k denotes the Von Karman Constant.

Over the land areas the roughness length Z_0 is defined as a function of the elevation h following Manobianco (1989), i.e.,

$$Z_0 = \{0.15 + 0.2 \times 10^{-8}(2368.0 + 18.42h)^2], \quad (4.10)$$

while over oceans the Charnock's formula is used, i.e.,

$$Z_0 = \frac{0.04 U^{*2}}{g} \quad (4.11)$$

The expression for C follows the analysis of Louis (1979):

$$C = \frac{7.4 \times 9.4 k^2}{[\ln(Z_2/Z_1)]^2}\left[\frac{Z_2}{Z_1}\right]^{1/2} \quad (4.12)$$

for momentum,

$$C = \frac{5.3 \times 9.4 k^2}{[\ln(Z_2/Z_1)]^2}\left[\frac{Z_2}{Z_1}\right]^{1/2} \quad (4.13)$$

for heat and moisture.

Here the following definition of the Bulk Richardson number is used:

$$\mathrm{Ri_B} \equiv \frac{g}{\bar{\theta}}\frac{(\theta_2 - \theta_1)(Z_2 - Z_1)}{(U_2 - U_1)^2}. \quad (4.14)$$

We shall next address the reverse similarity theory where one solves for θ_2 and q_2 given the surface fluxes of heat and moisture.

For a closure of the reverse similarity equation we assume that the wind at the lowest model level U_2 is known. Since heat flux defines the stability, the only unknown in the equations (4.5) and (4.8) is θ_2. Which can be solved directly or iteratively.

For the unstable case, where $U_*\theta_* < 0$, we define an objective function

$$F \equiv \frac{U_*\theta_*}{(U_2 - U_1)(\theta_2 - \theta_1)} + \frac{k^2}{0.74[\ln(Z_2/Z_1)]^2} \times \left(1 - \frac{9.4\,\mathrm{Ri_B}}{1 + C\,|\mathrm{Ri_B}|^{1/2}}\right). \quad (4.15)$$

Next we search for the value of θ_2 which minimizes F. Given a guess of θ_2^n and a tiny increment of θ_2^n, $\delta\theta_2$, $F(\theta_2^n + \delta\theta_2)$ and $F(\theta_2^n - \delta\theta_2)$ can be computed using eq. (4.15). One can also compute an approximation for the derivative of F with respect to θ_2, i.e.,

$$\left(\frac{\Delta F}{\Delta\theta_2}\right)^n = \frac{F(\theta_2^n + \delta\theta_2) - F(\theta_2^n - \delta\theta_2)}{2\,\delta\theta}. \quad (4.16)$$

Next an updated value of θ_2 can be computed from the Newton-Rhapson approach, i.e.,

$$\theta_2^{n+1} = \theta_2^n + \frac{F(\theta_2^n)}{-(\Delta F/\Delta\theta_2)^n} \quad (4.17)$$

This iterative procedure is continued to an accepted threshold value of $|\theta_2^{n+1} - \theta_2^n|$. Experiments show that the above scheme indeed converges extremely fast.

For stable conditions, eq. (4.5) may be written as

$$4.7^2\,\mathrm{Ri_B}^2 + (9.4 - A)\,\mathrm{Ri_B} + 1 = 0, \quad (4.18)$$

$$A = \frac{1}{0.74}\frac{\bar{\theta}}{g\,\Delta z}\frac{(U_2 - U_1)^3}{U_*\theta_*}\frac{k^2}{[\ln(Z_2/Z_1)]^2}. \quad (4.19)$$

It is easy to prove that the signs of both roots of

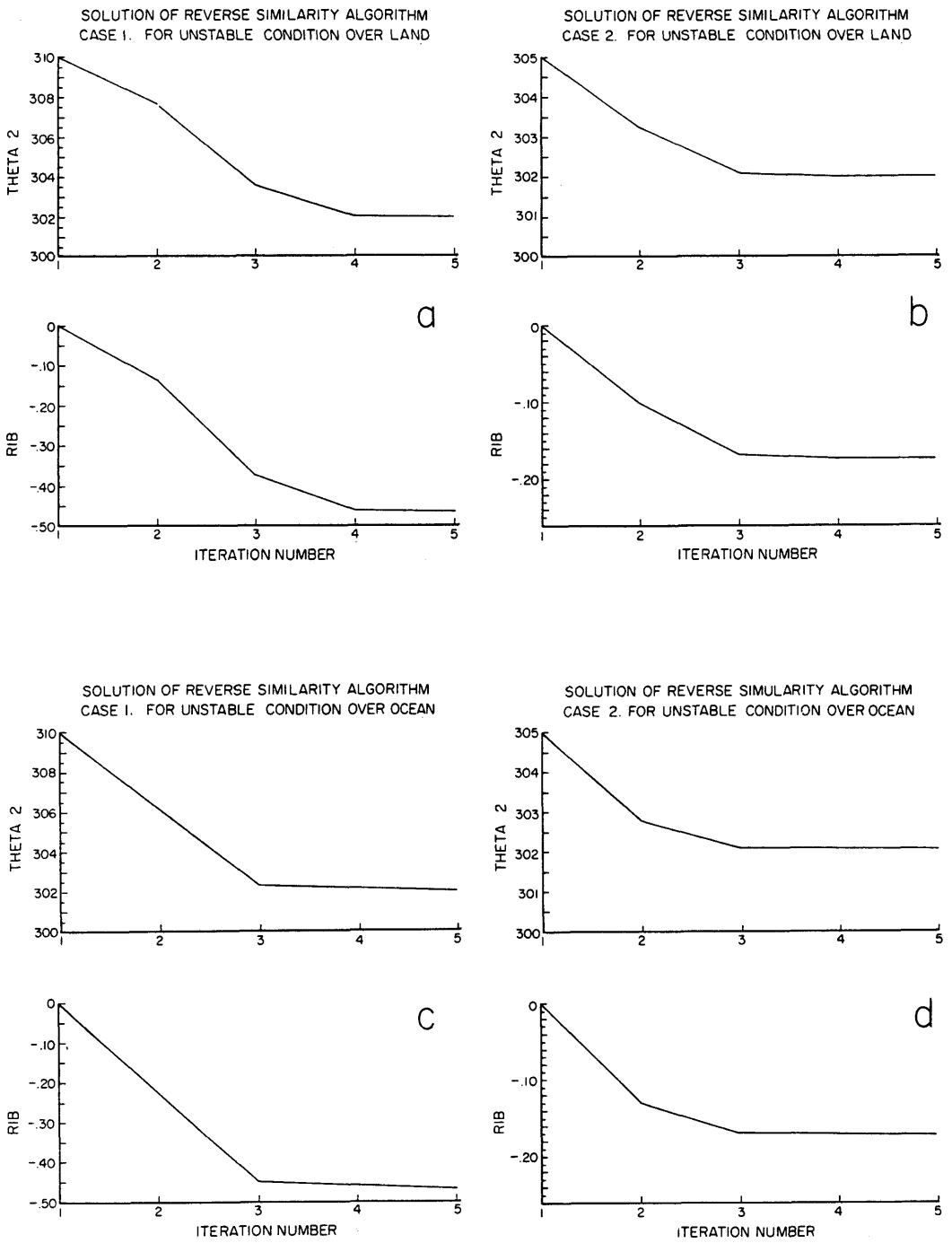

Fig. 5. The convergence of the potential temperature (°K) on top of the constant flux layer and of the Bulk Richardson number as a function of iterations for oceanic and land grid points.

(4.19) are positive and that the root with the larger value is beyond the physical upper limit of Ri_B. In other words, the solution should be the smaller root. θ_2 can be obtained from (4.14). Here the influence of the change of $\bar{\theta}$ is disregarded.

Once θ_2 is computed, C_H, C_q can be obtained using equations (4.5), (4.6), (4.8), and (4.9) and q_2 is obtained from equation (4.3).

4.1. Convergence of the reverse similarity theory

For the stable case the exact solution for θ_2 and q_2 are given by eqs. (4.5) and (4.6) and have no convergence problem.

For the unstable case the Newton Rhapson iteration provides a convergence to the prescribed Yanai fluxes within 3 to 4 iterations. The convergence is very rapid and accurate to roughly 1 W/m^2. Thus the Yanai fluxes are nearly exactly reproduced from the proposed reverse similarity theory. Fig. 5 illustrates the typical convergence at selected points for the unstable case over land and oceanic regions. Panel a (top) illustrates the convergence of the potential temperature and the bottom panel shows the convergence for the bulk Richardson number Ri_B. Only a few examples on convergence, over land and ocean, are illustrated here. The global convergence over all of the Gaussian grid points is easily attained for the unstable surface layers. The exact solution is, as stated above, possible for all of the stable surface layer points. In the global model, over all of the Gaussian grid points the convergence is met within 3 to 4 scans and the Yanai fluxes are recovered. In view of this we shall not illustrate the global distribution of the Yanai fluxes of sensible and latent heat and those obtained from the inverse similarity since they are identical over the entire globe.

5. Reverse cumulus parameterization

The vertical distribution of specific humidity is reanalyzed such that the rainfall implied by the cumulus parameterization algorithm closely matches the prescribed "observed" rainfall rates. The procedure for the construction of a reverse cumulus parameterization algorithm was discussed in Krishnamurti et al. (1984 and 1988b). This was designed for a modified Kuo's scheme that is described in Krishnamurti et al. (1983b). Similar reverse cumulus parameterization algorithms have been proposed by Donner (1988).

In our formulation the modified Kuo's scheme invokes two parameters b and η; b is a moistening parameter and η is a mesoscale convergence parameter. The large scale moisture supply is defined by

$$I_L = -\frac{p_s}{g}\int_{\sigma=\sigma_T}^{\sigma=\sigma_B} \dot{\sigma}\frac{\partial q}{\partial \sigma}\,d\sigma, \tag{5.1}$$

where σ_B and σ_T denotes a sigma surface at the cloud base and cloud top, respectively. The total supply is denoted by

$$I = I_L(1+\eta). \tag{5.2}$$

The total moistening and rainfall rates are expressed by the relations,

$$M = I_L(1+\eta)b, \tag{5.3}$$

$$R = I_L(1+\eta)(1-b). \tag{5.4}$$

The modified Kuo's scheme makes use of a multiple regression to optimize the heating, moistening and rainfall rates. Here, M and R are expressed as functions of several large scale variables that have a strong control on deep convection. Thus the evolving large scale variables of a forecast determine the local values of M and R which in turn determine b and η and thus a closure of the parameterization was accomplished. For further details on this method, reference may be made to Krishnamurti et al. (1983b and 1988b). An earlier version of a modified Kuo's scheme was based on the choice of parameters,

$$b = 0, \tag{5.5}$$

$$\eta = 0. \tag{5.6}$$

This was tested in a semiprognostic frame using data sets from the ships of the GATE experiment. Basically these tests showed that the rainfall rates and the heating rates were reasonably defined from this choice of values for the parameters b and η, although this scheme did not permit any moistening. It is a relatively straight forward exercise to write down a reverse Kuo algorithm for this choice of parameters and for a given rainfall rate.

The moisture availability is again expressed by the relation,

$$I_L = -\frac{p_s}{g}\int_{\sigma=\sigma_T}^{\sigma=\sigma_B} \dot{\sigma}\frac{\partial q}{\partial \sigma}\,d\sigma. \tag{5.7}$$

In the reverse Kuo, the specific humidity q is modified using the relation,

$$q_m = \frac{R\cdot q}{-\frac{p_s}{g}\int_{\sigma_T}^{\sigma_B}\dot{\sigma}\frac{\partial q}{\partial\sigma}\,d\sigma} + \frac{\frac{1}{g}\int_{\sigma_T}^{\sigma_B} q\,d\sigma}{\frac{1}{g}\int_{\sigma_T}^{\sigma_B} d\sigma} \times\left[1-\frac{R}{-\frac{p_s}{g}\int_{\sigma_T}^{\sigma_B}\dot{\sigma}\frac{\partial q}{\partial\sigma}\,d\sigma}\right]. \tag{5.8}$$

Here q_m is the modified specific humidity, q is the specific humidity prior to modification, R is the *observed* rainfall rate, the remaining are standard symbols explained in Appendix A.

The moisture convergence corresponding to the modified specific humidity matches the observed rainfall which is given by the relation,

$$-\frac{p_s}{g}\int_{\sigma_T}^{\sigma_B}\dot{\sigma}\frac{\partial q_m}{\partial\sigma}\,d\sigma = R. \tag{5.9}$$

The total precipitable water remains an invariant, i.e.,

$$\frac{1}{g}\int_{\sigma_T}^{\sigma_B} q_m\,d\sigma = \frac{1}{g}\int_{\sigma_T}^{\sigma_B} q\,d\sigma. \tag{5.10}$$

The limitations of the matching are obvious, i.e., if in a region where $R>0$, the supply I_L can be zero or negative, this method would not work. Furthermore, saturation is imposed as a limit, i.e., q_m cannot exceed q_s (the saturation value) thus an exact match is not possible in regions of excessive rain-

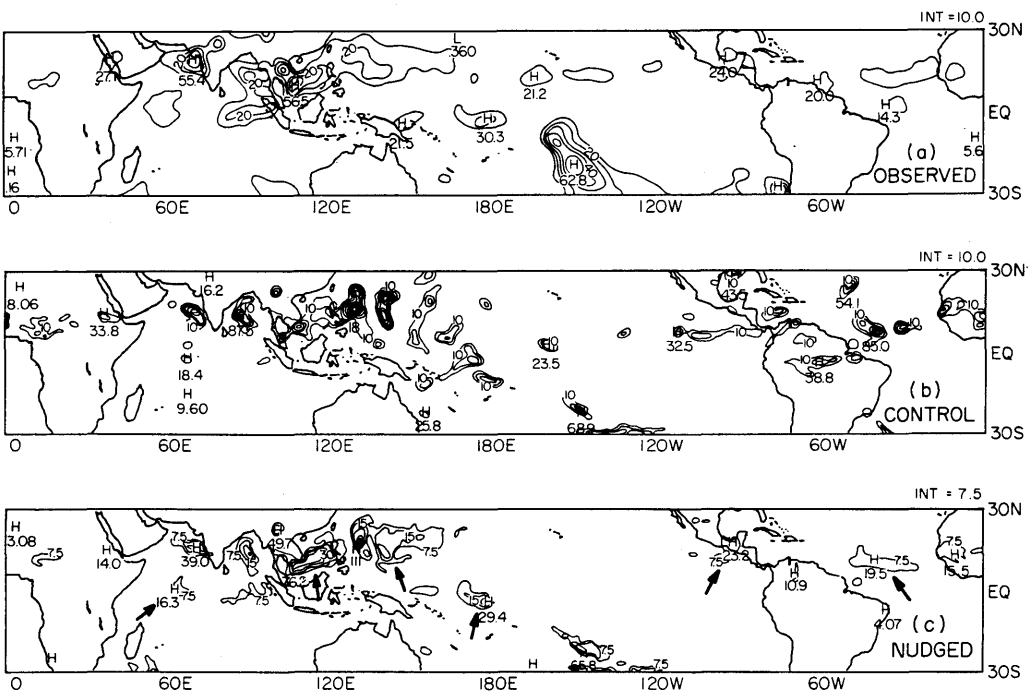

Fig. 6. An example of precipitation initialization (from 26 July to 27 July 1979, 12 UTC), 10 mm/day. (a) Based on satellite raingage observations. (b) Based on a control experiment first time step rainfall rates. (c) Based on Newtonian relaxation experiment from day −1 to day 0.

fall by this procedure. Here we shall illustrate an example of tropical rainfall distribution from (a) *observed*, (b) use of cumulus parameterization from the control analysis of humidity and (c) use of cumulus parameterization from the modified analysis of the humidity. Fig. 6 illustrates typical distribution of these three fields for 26 to 27 July 1979 (12 UTC).

The reverse cumulus parameterization is only applied to the tropical latitudes between 30°S and 30°N. Elsewhere a smooth transition to the control values (i.e., unadjusted) are retained beyond 35°S and 35°N. The calculations shown in Figs. 6b, c illustrate a major improvement from the use of the reverse cumulus parameterization algorithm in the data spare tropics. The arrows in Fig. 6c identify regions where the control experiment failed to specify the initial rainfall where improvements were possible from the use of this procedure. This illustration is a snapshot view of the reverse cumulus parameterization and the matching of rainfall. It should be noted that this procedure is not sufficient for the improvement of numerical weather prediction, this was also noted by Puri and Miller (1990). It is necessary to assimilate the related condensation heating and the spinup of the divergent wind to the model's initial state. That is accomplished by a Newtonian relaxation of the humidity field during a pre-integration phase prior to day 0 of the forecast where the interpolated rainfall is subjected to the reverse cumulus parameterization at each time step. The moisture and the related heating field exert their influence on the divergence field which is initialized in a consistent manner. The Newtonian relaxation is described in Section 7.

6. Initialization of the earth's radiation budget

It is possible to produce a close match between the outgoing long wave radiation as inferred by the polar orbiting satellite and as determined from the model's radiation algorithm. The humidity measurements above the 500 mb surface from the conventional radiosonde is generally quite unreliable. Locally, a structure function for the moisture variable, above the 500 mb, can be defined using a single parameter ε. The local difference between the two estimates of OLR (satellite versus model) can be minimized, thus determining an optimal value of ε. This procedure tends to improve the high and the middle clouds and the planetary albedo and thus resulting in an overall improvement of the earth's radiation budget. This is not a unique method since a matching of OLR can in principle be accomplished by altering the cloud fractions. In principle infinitely many possible combinations of low, middle, and high clouds can provide this matching.

The humidity analysis entails an iterations procedure; thus for an iterations l we write

$$q_l = q_{l-1}(1+\varepsilon) \tag{6.1}$$

where for $l=0$, $q_0 = q$ (analysis).

Let

$$\delta = \mathrm{OLR_M} - \mathrm{OLR_{SAT}}, \tag{6.2}$$

where the subscript M denotes the model based value and SAT denotes the satellite based value. A tolerance value of 10 W/m^2 for $|\delta|$ was assigned, i.e., if $|\delta| < 10$ W/m^2, the iteration is discontinued.

If

$$\delta_{l-1} \cdot \delta_{l-2} > 0, \tag{6.3}$$

i.e., when either

$$\mathrm{OLR_{M}}_{l-1} > \mathrm{OLR_{SAT}}$$

and

$$\mathrm{OLR_{M}}_{l-2} > \mathrm{OLR_{SAT}}$$

or

$$\mathrm{OLR_{M}}_{l-1} < \mathrm{OLR_{SAT}}$$

and

$$\mathrm{OLR_{M}}_{l-2} < \mathrm{OLR_{SAT}},$$

then we define

$$F_{l-1} = F_{l-2}$$
$$\varepsilon_l = R_{l-1} \cdot 0.01 \cdot F_{l-1} \tag{6.4}$$

and we set

$$q_l = q_{l-1}(1+\varepsilon_l). \tag{6.5}$$

Tellus A-B/43/4-5

If

$$\delta_{l-1} \cdot \delta_{l-2} < 0, \tag{6.6}$$

i.e., when either

$$OLR_{Ml-1} > OLR_{SAT}$$

and

$$OLR_{Ml-2} < OLR_{SAT}$$

or

$$OLR_{Ml-1} < OLR_{SAT}$$

and

$$OLR_{Ml-2} > OLR_{SAT},$$

then we define

$$F_{l-1} = 0.5 F_{l-2}$$

$$\varepsilon_l = R_{l-1} \cdot 0.01 \cdot F_{l-1} \tag{6.7}$$

and set

$$q_l = q_{l-1}(1 + \varepsilon_l). \tag{6.8}$$

Here, $R_{l-1} = OLR_{SAT} - OLR_{Ml-1}$, the residue at the end of interation $l-1$. An initial value of a convergence factor F is set to 1.0.

Iteration of eqs. (6.2) through (6.8) exhibits a rapid convergence in roughly 4 scans. A match of the model based OLR to the satellite based values within 10 W/m^2 is realized by this bisection procedure. Here we shall illustrate two examples for this initialization procedure. Fig. 7 illustrates the tropical distribution of OLR. The three respective panels show the satellite based, the model based (control), and the model based (after initialization) values. These were calculated for a model resolution of T42. Fig. 8 illustrates a second example which was initialized for the resolution T106. Basically, a very close matching of OLR is indeed realized. The correlation coefficient between the satellite based and initialized OLR is of the order of 0.95 while that for the satellite based and the

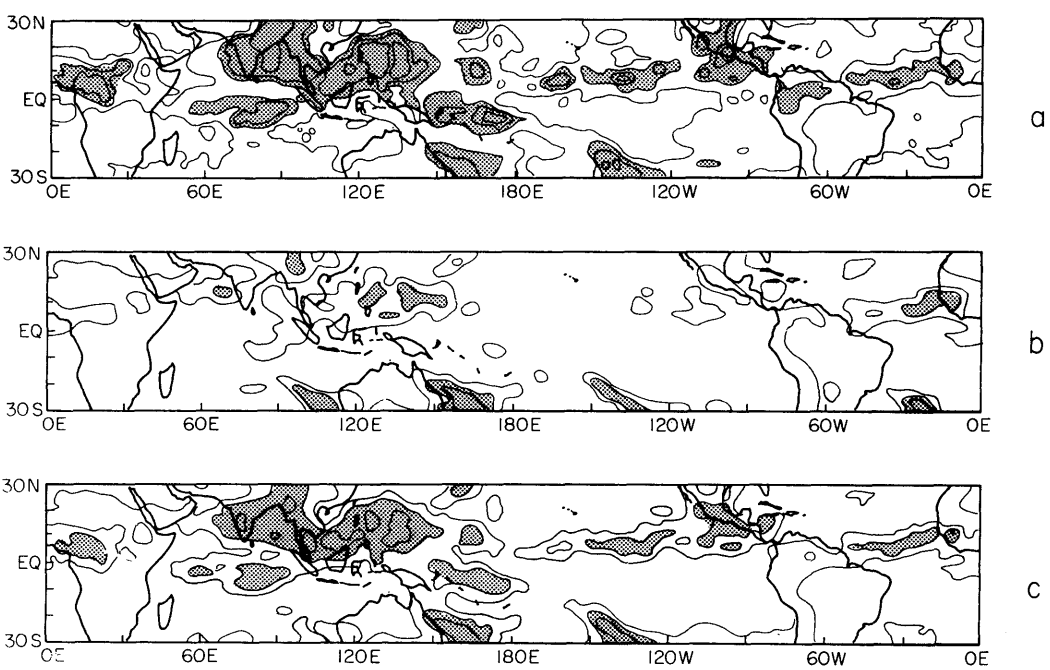

Fig. 7. Field of the initial outgoing long-wave radiation, (27 July 1979) (W/m^2). Interval of analysis 40 W/m^2, shaded area denotes values less than 240 W/m^2. (a) Based on polar orbiting satellite data sets. (b) Based on a control experiment forecast at a resolution T42. (c) Based on the Newtonian relaxation experiment at a resolution T42.

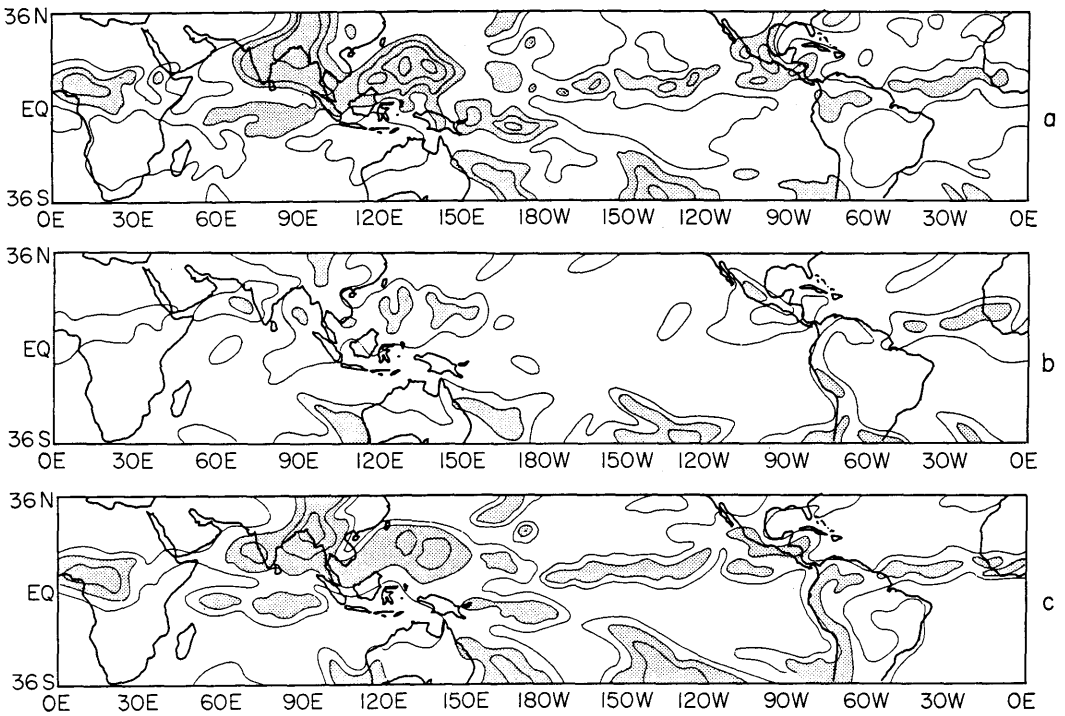

Fig. 8. Field of the initial outgoing long-wave radiation, (27 July 1979) (W/m^2). Interval of analysis 40 W/m^2, shaded area denotes values less than 240 W/m^2. (a) Based on polar orbiting satellite data sets. (b) Based on a control experiment forecast at a resolution T106. (c) Based on Newtonian relaxation experiment at a resolution T106.

control is of order of 0.4. The initial humidity analysis in the upper troposphere is thus constrained to the matching of the OLR. The limitation of this method were stated earlier.

7. Newtonian relaxation

Also termed as nudging, (Hoke and Anthes, 1976), this is a powerful technique for the initialization of physical processes. It is possible to introduce the notions of physical initialization, as proposed in the earlier sections. This will be carried out using a Newtonian nudging of the basic variables of the model during a preintegration phase. Some of the variables will be strongly relaxed in comparison to others. This has to do with overall distribution of observations in the tropics and for the need to improve the regional and global spin up. The vorticity, divergence and the pressure tendency equations are subjected to a Newtonian relaxation. The spectral equations take the form,

$$\frac{\partial A_l^m}{\partial t} = F_l^m(A, t) + N(A, t) \cdot (A^{\circ m}_l - A_l^m). \qquad (7.1)$$

Here N denotes the relaxation coefficient, $A^{\circ m}_l$ represents a future value to which the Newtonian relaxation is aimed at. $F_l^m(A, t)$ is a forcing term of the equations for a variable A_l^m. The integrations are carried out in two steps, the tendencies for the normal forcing terms F_l^m are first carried out. The Newtonian term is expressed in finite difference form using the relation;

$$\frac{A_l^m(t+\Delta t) - A^{*m}_l(t+\Delta t)}{2\,\Delta t} = N(A, t)[A^{\circ m}_l(t+\Delta t) - A_l^m(t+\Delta t)] \qquad (7.2)$$

or

$$A_1^m(t+\Delta t) = (A^{*m}_1(t+\Delta t) + 2\,\Delta t \cdot N(A,t) \cdot A^{\circ m}_1(t+\Delta t))/(1+2\,\Delta t \cdot N(A,t)). \quad (7.3)$$

Here $A^{*m}_1(t+\Delta t)$ denotes a predicted value of A_1^m at time $(t+\Delta t)$ prior to the Newtonian relaxation. It is clear that the value of the variable A_1^m in the relaxation process is a weighted average of the model predicted and the "observed" value and thus is falls between these values as the relaxation proceeds. Following Krishnamurti, et al. (1988c) the relaxation coefficients were kept time invariant, their values were simply determined from numerical experimentation. The following values were used:

vorticity:	$N = 1 \times 10^{-4}\ s^{-1}$
divergence:	$N = 5 \times 10^{-5}\ s^{-1}$
surface pressure:	$N = 1 \times 10^{-4}\ s^{-1}$
humidity	(see below).

A lower value of N, for the divergence, is used to permit the impact of physical initialization. The divergence field evolves strongly from the imposed heating (the prescribed rainfall rates) and is weakly relaxed to the analysis.

During the preintegration phase the prediction of the humidity field consists of three steps:

(i) The humidity field at the lowest level ($\sigma = \sqrt{0.99}$) of the model is constructed from the reverse similarity theory. That calculation is carried out at intervals of every 12 h. During the preintegration phase between hours -24 to 0, the predicted humidity field at this level is relaxed (i.e., nudged) to these values. For the surface layer the relaxation coefficient $N = 5 \times 10^{-5}$.

(ii) The reverse cumulus parameterization is carried out at each time step during the preintegration phase. The humidity field thus obtained defines the predicted humidity field at the time step. No Newtonian relaxation of the humidity field is carried out above the constant flux layer.

(iii) Above the $\sigma = 0.5$ level, the humidity analysis is based on a matching of the outgoing longwave radiation described in Section 6. This overrides the humidity analysis above the $\sigma = 0.5$ level that was given by step (ii) i.e., the reverse cumulus parameterization. Ideally steps (ii) and (iii) require iterations; however, we noted that such iterations were not necessary since the above sequence suffice to provide an adequate initialization of clouds, rainfall, and surface fluxes.

The global model at the resolution T106 was used to carry out a control and a Newtonian relaxation experiment and then forecasts were carried out for the respective initializations. The relaxation showed a major improvement in the initialization of the following fields.

(a) The surface fluxes. A comparison of the control and Newtonian relaxation showed improvements. These will be discussed later.

(b) The precipitation field, likewise, shows a close agreement to the prescribed "observed" measures of the rainfall rates.

(c) The velocity potential field exhibits a spin up of the divergence field consistent with the imposed heating from the "observed" rainfall distributions.

(d) The initialization also shows an improvement in the overall cloud distribution as seen from the field of the outgoing long-wave radiation. That improvement from the Newtonian relaxation over what was obtained from the control is strikingly large (see Figs. 7, 8).

In spite of the care exercised in dealing with the surface fluxes, rain and OLR in the physical initialization this scheme does not assure a physically consistent vertical distribution of heating. During the Newtonian relaxation these imposed constraints provide a vertical distribution of heating which is consistent with the model algorithms such as the modified Kuo's scheme. That may depart from a "true heating profile" which cannot be attained due to the inherent modeling aspects. There we view the physical initialization as a procedure which makes maximum use of observations within the constraints of the forecast model.

8. Impact study on medium range forecasts over the tropics

Here we shall show examples of forecasts made at a resolution T106. The forecasts of the surface fluxes, precipitation and circulation at 850 mb are shown. The forecasts for the Newtonian relaxation and a control experiment are compared with the

analysis. The control experiment is a forecast starting on day 0 subsequent to a nonlinear normal mode initialization.

8.1. Predicted surface flux of moisture

The surface flux of moisture (expressed in units W/m^2) for days 1, 3 and 5 of predictions are illustrated in Figs. 9, 10 and 11. Each of these illustrations contains two panels, panel "a" shows the forecasts from the control experiment and panel "b" shows the results from the Newtonian relaxation experiment. Three features are clearly apparent in these forecasts. (1) The fluxes for the Newtonian relaxation experiment are about 50 to 100 W/m^2 higher than those for the control experiment over the region of the trade winds of the southern Indian ocean. (2) Another region of large moisture flux exceeding 200 W/m^2 is located over the Arabian sea along the Somali jet near 15° N. Here the fluxes from the Newtonian relaxation experiment are about 50 W/m^2 larger than those for the control experiment. (3) The fluxes around

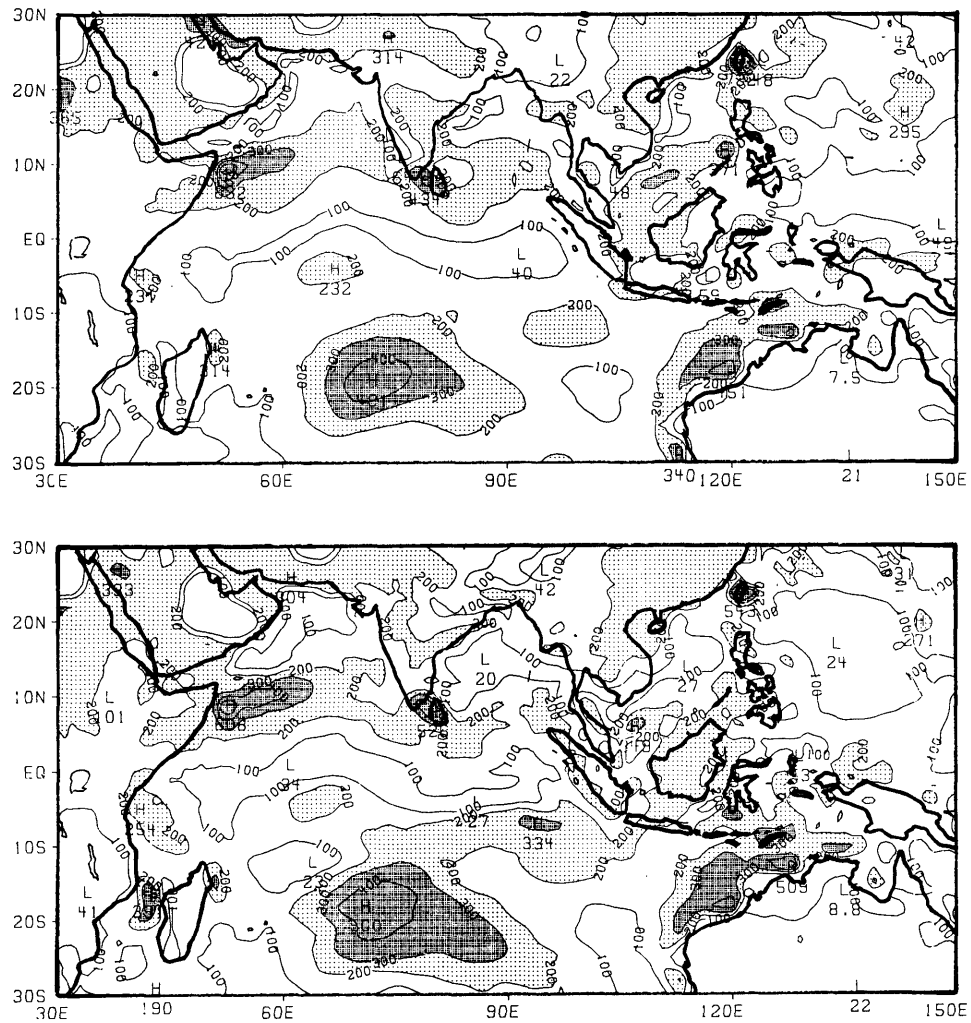

Fig. 9. The predicted surface flux of latent heat on day 1 (W/m^2). (27 July 1979, 12 UTC). (a) Top panel control experiment. (b) Bottom panel Newtonian relaxation experiment.

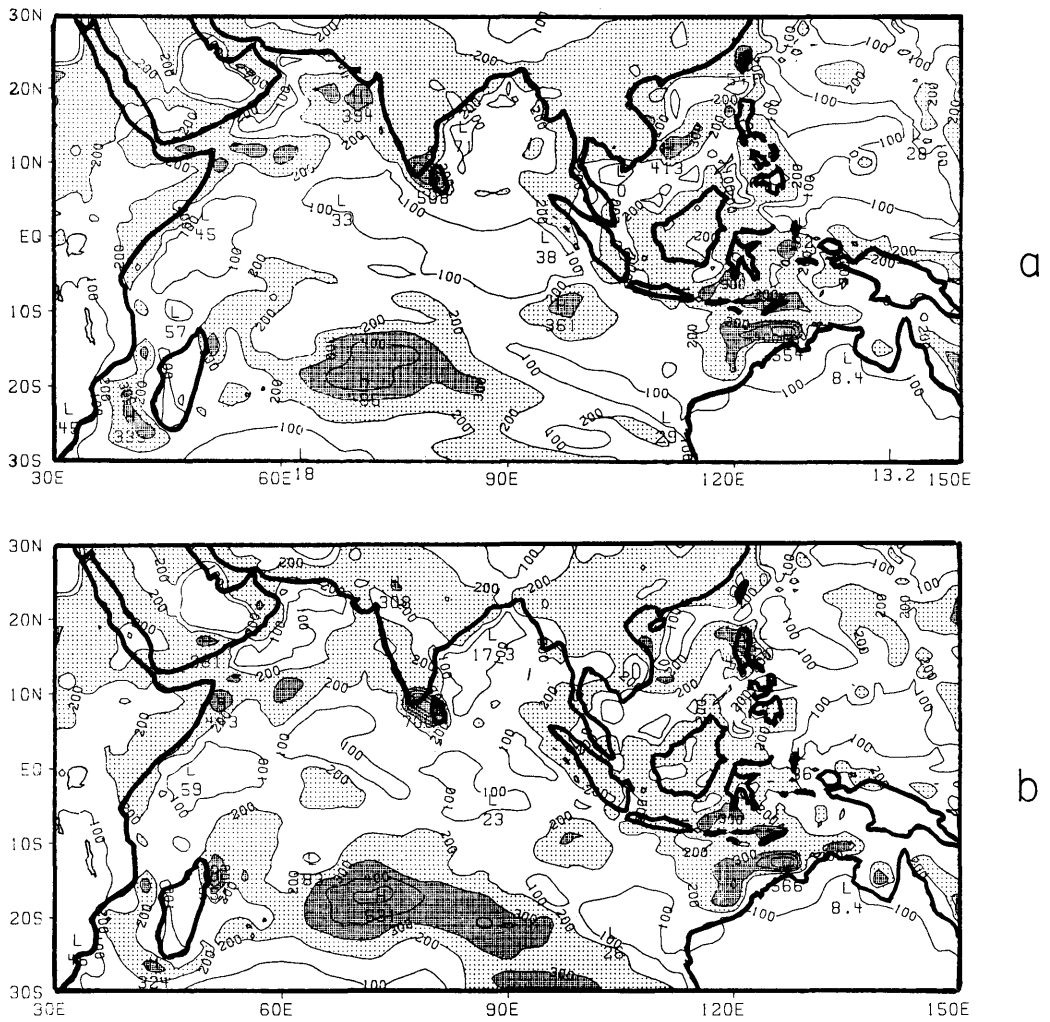

Fig. 10. The predicted surface flux of latent heat on day 3 (30 July 1979, 12 UTC) (W/m^2). (a) Top panel control experiment. (b) Bottom panel Newtonian relaxation experiment.

the typhoon show a marked organization. Fluxes exceeding 200 W/m^2 exhibit such an organization around the storm.

Since observational measures of detailed fluxes are lacking, a priori it would be difficult to state that the results shown above are indeed indicative of a strong impact from the proposed improvements in the initialization. However it is apparent that the fluxes from the proposed initialization experiment are most robust, and show a greater degree of organization along the trades, the monsoons and the typhoon. The larger evaporation through 5 days of prediction, from the Indian ocean and the Arabian sea, contributes to the sustained monsoon rainfall over India and Burma which persisted throughout this forecast period. The fluxes for the initialization experiment remain somewhat larger in magnitude and in a real coverage through days 4 and 5 of forecasts in comparison to the control experiment. We believe that this was a positive impact on the precipitation as well as the circulation forecasts.

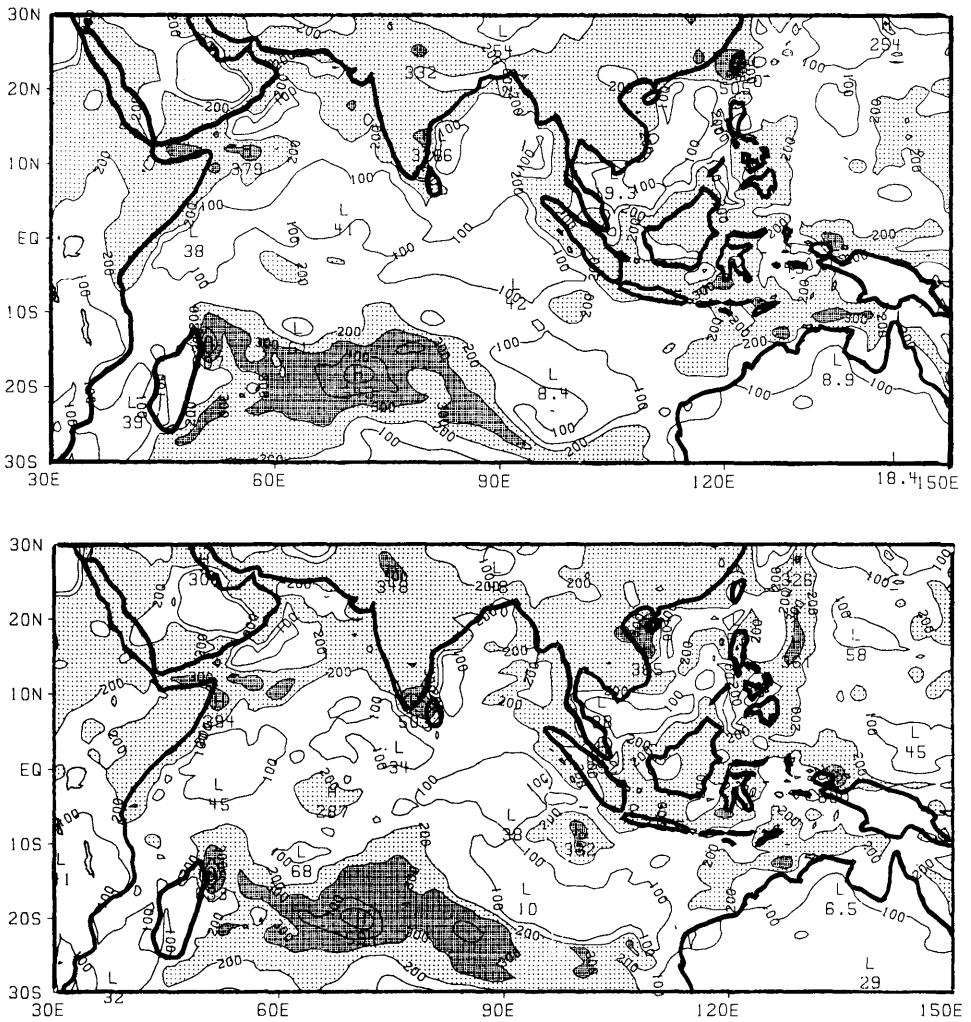

Fig. 11. The predicted surface flux of latent heat on day 5 (1 August 1979, 12 UTC) (W/m^2). (a) Top panel control experiment. (b) Bottom panel Newtonian relaxation experiment.

8.2. Precipitation forecasts

In Figs. 12 and 13, we illustrate the 24-h precipitation totals. Panel (a) shows the observed "i.e. based on satellite and raingage", panel (b) shows the forecasts from the control experiment and panel (c) shows the forecasts from the Newtonian relaxation. These illustrate the forecasts of rainfall amounts from days 0 to 1, and 4 to 5 respectively. There are several features of interest in the "observed" rainfall during this period. An axis of rainfall over the west coast of India, and along the west coast of Burma are persistent features. During the five day period a tropical depression formed over the Bay of Bengal and made its landfall along roughly 15°N. The storm was located inland by day 5 of forecast. The observed precipitation patterns on day 5 included heavy rainfall along the west coasts of India and Burma. In addition, during this period, typhoon Hope, in the Western Pacific ocean, was traversing towards Hong Kong. A broad zonal belt of rainfall shown

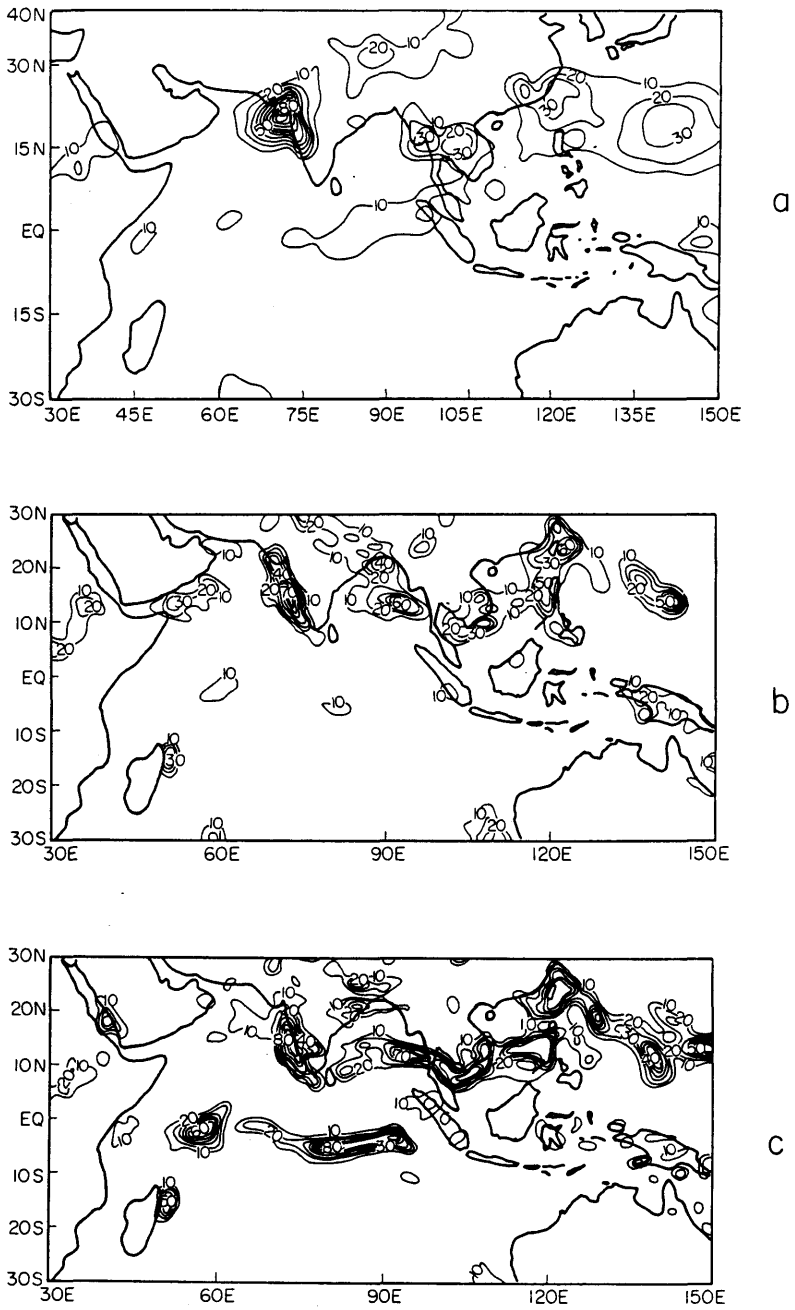

Fig. 12. The predicted precipitation field on day 1 (27–28 July 1979, 12 UTC) (mm/day). (a) Top panel based on satellite raingage observations. (b) Middle panel based on control experiment. (c) Bottom panel based on Newtonian relaxation experiment.

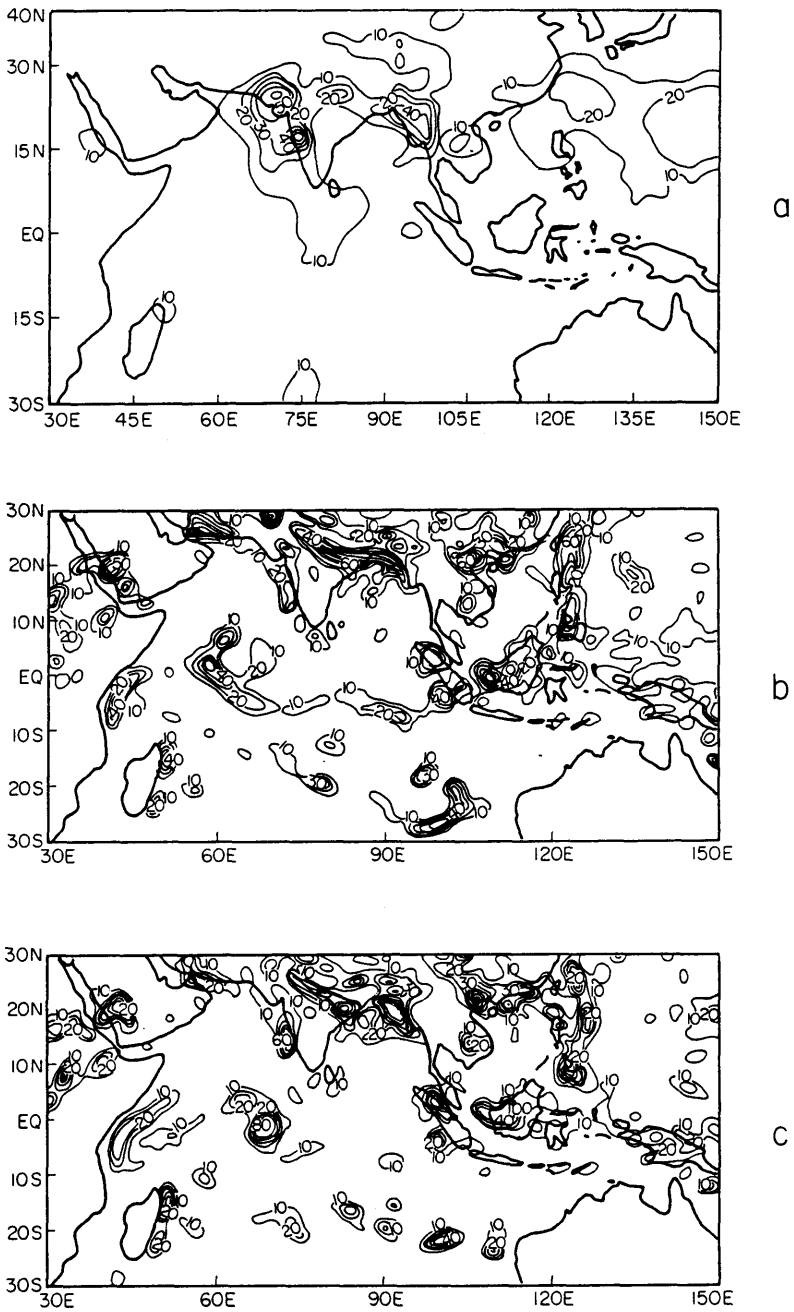

Fig. 13. The predicted precipitation field on day 5 (31 July to 1 August 1979, 12 UTC) (mm/day). (a) Top panel based on satellite raingage observations. (b) Middle panel based on control experiment. (c) Bottom panel based on Newtonian relaxation experiment.

in the "observed" panels for days 1 through 5 over the oceanic region along 20° N reflects some of the deficiencies in the estimates of rainfall intensity. The rainfall over this oceanic region is almost entirely based on satellite regression and this method appears to spread out the rainfall covering a broad region under the cirrus canopy. This deficiency is partly related to the resolution of the polar orbitor OLR data set used here, which was on a 2.5° latitude/longitude resolution. Some regions of apparent discrepancies are evident in the initialization. For instance, a region south of the equator, over the Indian Ocean, has recovered rain over the region of observed rain which was not handled by the control experiment. However, the intensity of the initialized rain is larger than the "observed" values. This may in part be due to the impact of the stronger evaporative flux over this region which was recovered by the model. Overall, the OLR based rainfall along this zonal belt is deficient over oceans (Krishnamurti et al., 1990). The impact of the predicted rainfall over coastal and the land areas is clearly apparent through day 5 of the forecast. The observed and predicted rainfall amounts for days 0 to 1 and 4 to 5, shown in Figs. 12 and 13, exhibit a rather large skill in rainfall prediction through day 5. The coastal rainfall, along the west coasts of India and Burma, is reasonably handled throughout this integration. Furthermore the inland rainfall during the passage of the monsoon depression are predicted extremely well. The rainfall amounts and locations of heavy rainfall for days 4–5 for the Newtonian relaxation experiment show a rather close agreement to the observed rainfall. The predicted oceanic rainfall amounts, lacking a better method for observational estimates, are hard to assess. However we feel that the land area predictions do seem to exhibit a small positive impact from the proposed initialization. We have examined the performance of this model for numerous other cases, Krishnamurti et al. (1990). Those experiments were also carried out at the resolution T106.

The 5-day mean predicted rainfall over the global tropical belt for the control and the Newtonian relaxation experiments are shown in Fig. 14. Lacking adequate observations over the oceans we shall not try to validate these with any proxy data. A comparison of the results of the two experiments shows the following: The ITCZ rainfall over the global oceans is much better defined and is stronger for the Newtonian relaxation experiment. The monsoon orographic rainfall is better defined for the Newtonian relaxation experiment. This may largely be consequence of slightly more accurate circulation forecasts for this experiment. The rainfall pattern over west Africa appears sharper and narrower, i.e. less wide spread for this

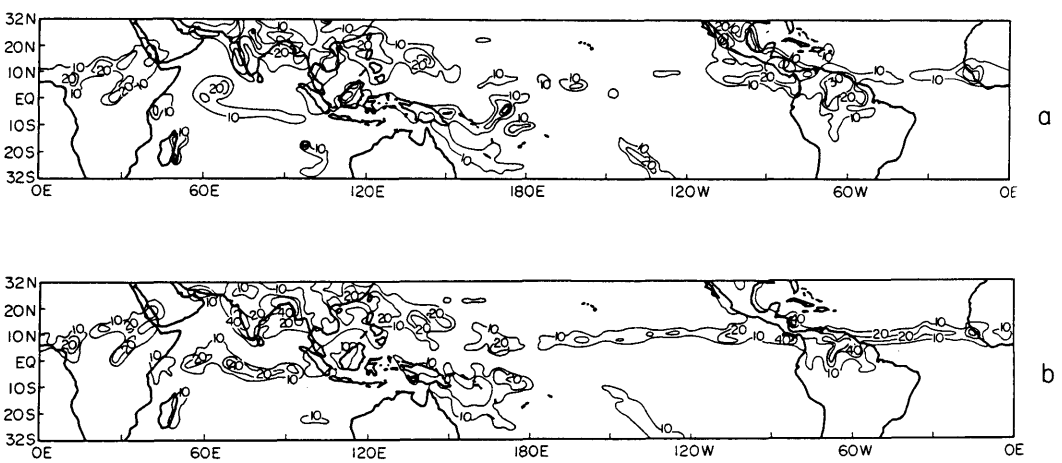

Fig. 14. Predicted 5-day mean rainfall on days 0 to 5 (27 July to 1 August 1979, 12 UTC) (mm/day). Top panel: control experiment. Bottom panel: Newtonian nudging experiment.

experiment. The passage of typhoon Hope leaves a large zonal region of heavy rain over the Western Pacific near 15 to 20°N. That appears to be handled slightly better by the Newtonian relaxation experiment.

8.3. *Circulation forecasts*

Figs. 15, 16 and 17 show the 850 mb circulation forecasts for days 1, 3 and 5. Here, the top panel shows the analysis, the middle panel shows the

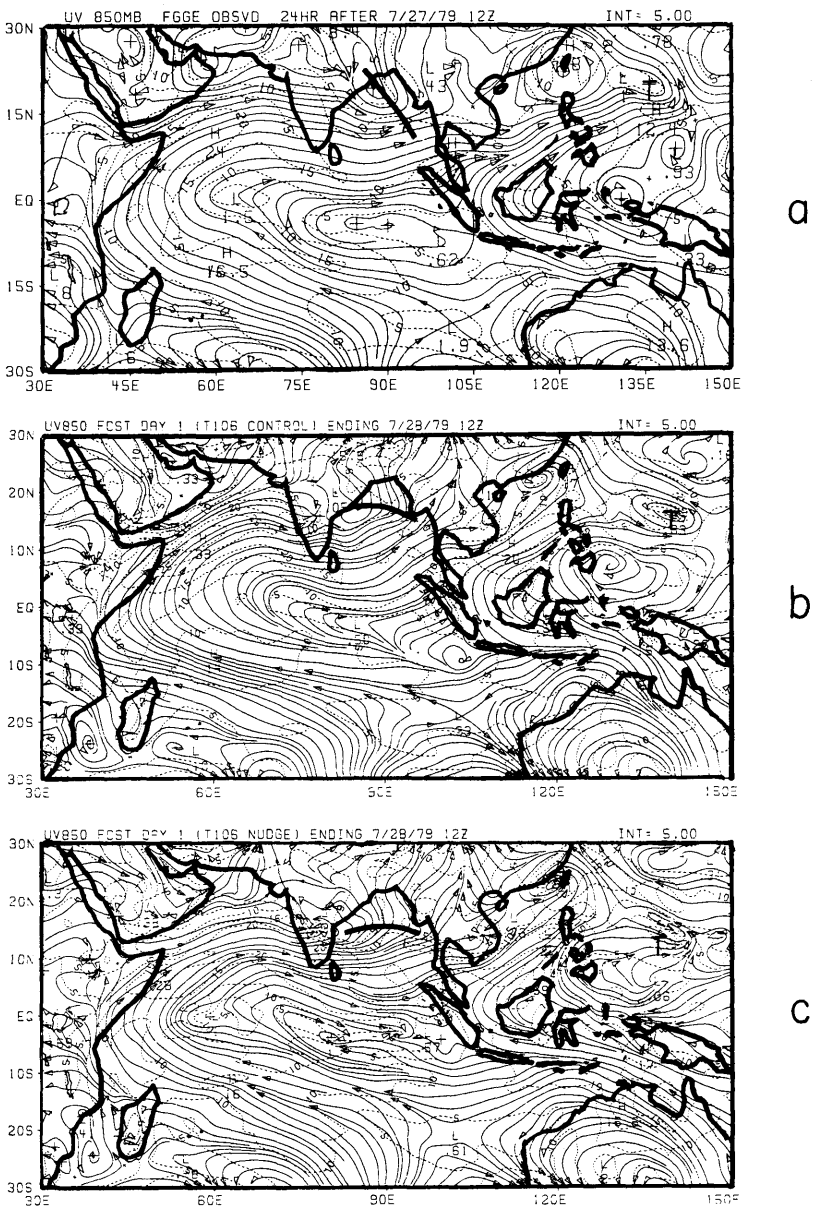

Fig. 15. Predicted streamlines and isotachs (dashed line, m/s) at 850 mb for day 1 (28 July 1979, 12 UTC). Top panel: analysis; middle panel: control experiment; bottom panel: Newtonian relaxation experiment.

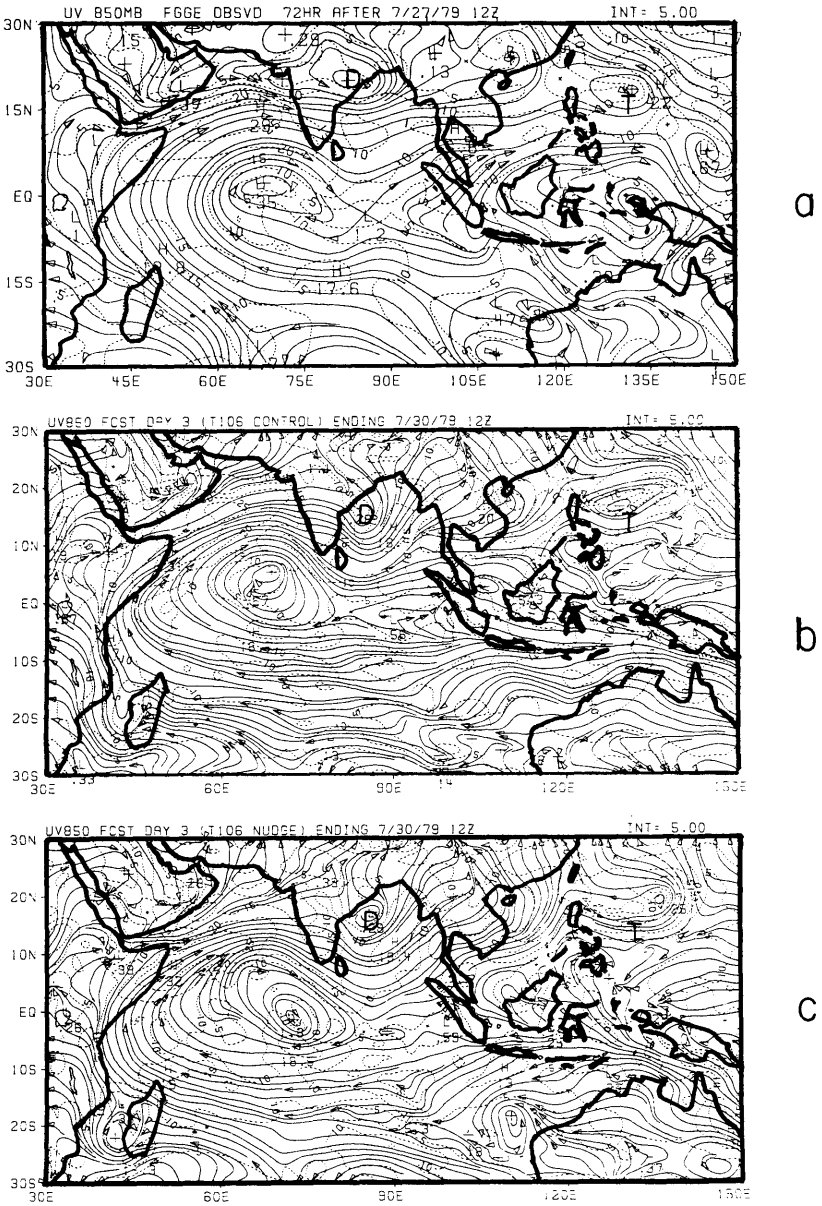

Fig. 16. Predicted streamlines and isotachs (dashed line, m/s) at 850 mb for day 3 (30 July 1979, 12 UTC). Top panel: analysis; middle panel: control experiment; bottom panel: Newtonian relaxation experiment.

control experiment forecasts and the bottom panel shows the Newtonian relaxation forecasts. In these illustrations, the depressions are marked by a letter D, the typhoon by the letter T and the trough line by a heavy black line.

The formation and landfall of the monsoon depression and the westward motion of typhoon Hope in the western Pacific are both handled reasonably well. The monsoonal circulation and the trades of the southern Indian Ocean are described extremely well by both models throughout these integrations. The forecast of the

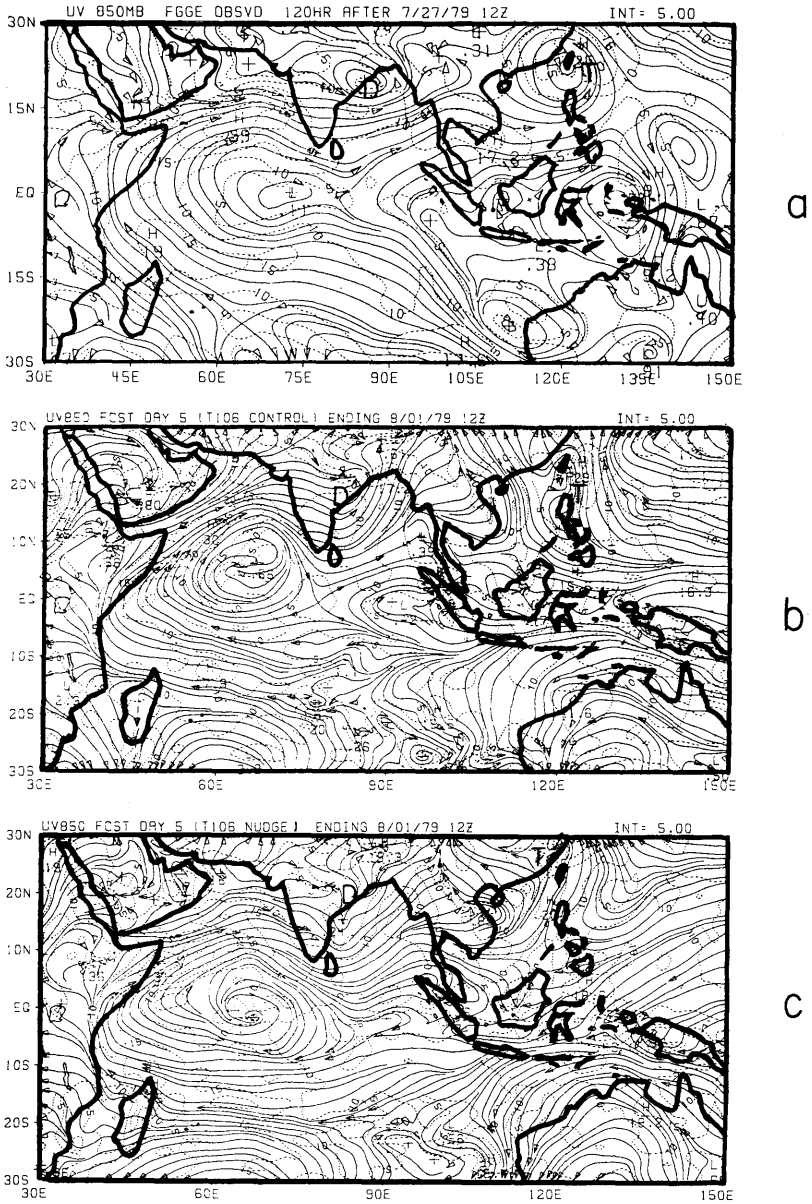

Fig. 17. Predicted streamlines and isotachs (dashed line, m/s) at 850 mb for day 5 (1 August 1979, 12 UTC). Top panel: analysis; middle panel: control experiment; bottom panel: Newtonian relaxation experiment.

near equatorial clockwise eddy extending across the Indian ocean is handled well by both models through day 5 of forecasts. This is a major feature over this region. The strength of the Somali jet and of the typhoon are handled slightly better by the Newtonian relaxation experiment in comparison to the control. Overall, the quality of these monsoon circulation forecasts shows a major improvement over what we had obtained from earlier versions of the model forecast for the same storms at the resolution T106, see Krishnamurti et al. (1990). It is worth noting that the overall changes

in the circulation patterns are not altered substantially by the proposed physical initialization. This is due to the stronger Newtonian relaxation of the rotational part of the wind at all vertical levels. The divergent part of the wind, a smaller fraction of the total wind, responds to the imposed precipitation heating and is altered significantly during the physical initialization.

9. Concluding remarks

Some 10 years from now, the promise of EOS includes a space based observing system that can enhance the global coverage of winds, temperature, humidity and rainfall measurements. An unprecedented improvement in the observational coverage over the tropics and the southern hemisphere is expected. It is difficult to assess how numerical weather prediction models would assimilate these data sets. It is conceivable that newer techniques to assimilate and initialize such a rich data base would be exploited. The availability of in situ Tropical Rainfall Measurements Mission (TRMM) provides the opportunity for a more detailed formulation of initialization for the tropical latitudes where the role of deep convection and associated heating is most important.

The distribution of the current upper-air radiosonde network over the tropical belt places a major limitation on the useful description of the state of the atmosphere. In this study, we have carried out a preliminary study to demonstrate the usefulness of some satellite products to enhance the World Weather Watch through the use of a physical initialization procedure. This procedure basically makes use of detailed data sets of the outgoing longwave radiation. That along with the currently available tropical raingage data sets are used to define the precipitation field. The initial surface fluxes are determined from vertical integrals of the apparent moisture sink and the apparent heat source distributions. These make use of the precipitation fields which are further used to determine a consistent vertical structure of the humidity field from the use of a reverse similarity and a reverse parameterization algorithm. The humidity analysis in the upper troposphere is structured to the satellite based outgoing longwave radiation. A Newtonian relaxation procedure initializes the surface fluxes, rainfall rates and the outgoing longwave radiation. This procedure is shown to initialize the surface fluxes to within 1 W/m^2 (i.e., the reverse similarity and the Yanai fluxes converge to this degree of accuracy).

It should be noted that this entire procedure can only be as good as what one sets out to start with, i.e., the Yanai fluxes. Any errors in the integral estimates of Yanai fluxes are simply conveyed to the initial state by this procedure. The accuracy of rainfall estimates is crucial for the determination of surface moisture fluxes in the rain areas. Since rainfall rates are expected to be in error by as much as 100% in heavy rain areas that will be reflected in the proposed initialization. The reverse cumulus parameterization seems to recover the prescribed rainfall rate to within 5 mm/day in regions of heavy rainfall intensity. Here errors in the humidity analysis generally result from an underestimation of heavy rainfall. By far the promising aspect of this initialization was found in the structuring of the humidity analysis to the satellite based values of the outgoing longwave radiation. That matching is possible to an accuracy of roughly 10 W/m^2. Although the uniqueness of this approach is open to question, this is shown to have a major impact in the prediction of the outgoing longwave radiation.

The Newtonian relaxation was seen to capture most of the prescribed information on the surface fluxes, the rainfall distribution and the field of the outgoing longwave radiation (i.e., the clouds). In the forecast experiments we have compared the results of a control experiment (which simply starts from day 0, subsequent to a nonlinear normal mode initialization) with the Newtonian relaxation experiment (which started on day -1). The comparison shows that the Newtonian relaxation experiment performed somewhat better through day 5 of the forecast in the following respects.

(a) The surface flux of moisture was stronger and better organized along the trade winds, monsoonal flows and the typhoon.

(b) Precipitation forecasts exhibited a better definition of the ITCZ along the entire global tropical belt.

(c) During this entire period, rainfall was persistent along the west coasts of India and Burma. The forecast was able to maintain these features

quite well through the 5 days, as was noted in the observations.

(d) The forecast of inland rainfall over India on day 5 exhibited a zonal belt of precipitation near 20°N. The Newtonian relaxation experimented predicted this feature quite close to the observed estimates.

It should be possible to improve the reverse cumulus parameterization further to include the effects of moistening, mesoscale convergence and clouds. Improvement in the resolution of the global model and the satellite data sets should be possible in the future.

During this decade, prior to the launch of the EOS platforms, the use of SMMI data sets holds much promise. This data set can be used to deduce the global coverage of precipitable water and rainfall rates, and thus appears to be ideal for extension of studies on physical initialization. It has a much higher resolution, i.e., of the order of 30 km, as compared to the 250 km resolution OLR data sets used in the present study.

The future satellite missions are mainly designed for providing data sets for the Global Change initiatives, their usefulness for climatic time scales is apparent in their desing. It remains to be seen if useful information can be extracted from these for the NWP problems.

The use of an adjoint of a numerical prediction model is considered as a major new avenue for addressing the spin-up and the initialization issues, Talagrand and Courtier (1987). The adjoint projects the model and the data errors in the redefinition of an initial state. Several weather centers (ECMWF, NMC and the LMD) are currently exploring this avenue. This approach may be a viable and more consistent substitute for the proposed physical initialization via Newtonian relaxation.

10. Acknowledgements

The senior author of this paper was invited to present this talk at the Bolin 65 Anniversary at the University of Stockholm. We wish to convey our deepest respects and gratitude to Professor Bert Bolin. He inspired us in the area of numerical weather prediction in the 1950s. His many contributions have paved the way for the development of this field. We are indebted to Ms. Rosemarie Raymond, Ms. Terri Lapido and Ms. Sara Meador for technical assistance in the preparation of this work. The research reported here was supported equally by two grants to the Florida State University, NSF Grant No. ATM-8812053 and Navy Grant No. N00014-J-89-1476. The computations for this work were carried out on the National Center for Atmospheric Research Cray X-MP/48 computer. The authors acknowledge the Supercomputer Computations Research Institute at Florida State University for facilities used in the production of graphics.

11. Appendix A

A list of acronyms and useful symbols

	Acronyms
AIRS	Atmospheric Infrared Radiation Sounder
ECMWF	European Center for Medium Range Forecasts
EOS	Earth Observing System
FGGE	First GARP Global Experiment
LAWS	Laser Atmospheric Wind System
LMD	Laboratoire de Météorologie Dynamique
NMC	National Meteorological Center
OLR	Outgoing Longwave Radiation
RAOB	Radiosonde Observation
SSMI	Special Sensor Microwave Imager
TRMM	Tropical Rainfall Measurement Mission
WWW	World Weather Watch

	Symbols
A_1^m	spectral coefficient of order m and degree 1
b	moistening parameter
C_H, C_q, C_M	exchange coefficient for heat, moisture and momentum
C_p	specific heat at constant pressure

F_S, F_L	surface fluxes of sensible and latent heat
F_H, F_Q, F_M	surface fluxes of sensible, latent heat and momentum
F	convergence factor
g	gravity
g_w	ground wetness parameter
I	total moisture convergence
I_L	large scale moisture convergence
k	Von Karman constant
L	latent heat of vaporization; Monin–Obukhov length
M	part of moisture convergence which moistens the atmosphere
N	nudging coefficient
P	pressure; precipitation
P_s	pressure at the earth's surface
q	specific humidity
q_m	modified specific humidity
Q_1	apparent heat source
Q_2	apparent moisture sink
Q_R	radiation heating
R	part of moisture convergence which precipitates; rainfall rate
Ri_B	bulk Richardson number
s	dry static energy
U_1, θ_1, q_1; U_2, θ_2, q_2	wind, potential temperature and specific humidity at the bottom and the top of constant flux layer
U_*, θ_*, q_*	characteristic frictional wind, potential temperature and specific humidity
Z_0	roughness parameter
Z_1, Z_2	height of the bottom and the top of the constant flux layer
σ	dimensionless vertical coordinate p/p_s
$\dot{\sigma}$	$d\sigma/dt$
σ_B, σ_T	σ values at bottom and top of convective cloud
η	mesoscale convergence parameter
$(\hat{\cdot})$	vertical integral operator
$(\bar{\cdot})$	horizontal average operator

Appendix B

Brief outline of the global spectral model

(a) Independent variables: (x, y, σ, t).

(b) Dependent variables: vorticity, divergence, surface pressure, vertical velocity, temperature and humidity.

(c) Horizontal resolution: triangular 106 waves.

(d) Vertical resolution: 12 layers between roughly 100 and 1000 mb.

(e) Semi-implicit time differencing scheme.

(f) Envelope orography (Wallace et al., 1983).

(g) Centered differences in the vertical for all variables except humidity which is handled by an upstream differencing scheme.

(h) Fourth-order horizontal diffusion (Kanamitsu et al., 1983).

(i) Kuo-type cumulus parameterization (Kuo 1965, 1974; Krishnamurti et al., 1983b).

(j) Shallow convection (Tiedke et al., 1988).

(k) Dry convective adjustment.

(l) Large-scale condensation (Kanamitsu, 1975).

(m) Surface fluxes via similarity theory (Businger et al., 1971).

(n) Vertical distribution of fluxes utilizing diffusive formulation where the exchange coefficients are functions of the Richardson number (Louis, 1979).

(o) Long- and short-wave radiative fluxes based on a band model (Lacis and Hanson, 1974; Harshvardan and Corsetti, 1984).

(p) Diurnal cycle.

(q) Parameterization of low, middle and high clouds based on threshold relative humidity for radiative transfer calculations.

(r) Surface energy balance coupled to the similarity theory (Krishnamurti et al., 1987).

(s) Nonlinear normal mode initialization, 5 vertical modes, (Kitade, 1983).

REFERENCES

Arkin, P. A. 1979. The relationship between fractional coverage of high cloud and rainfall accumulation during GATE over the B-scale array. *Mon. Wea. Rev. 107*, 1382–1387.

Businger, J. A., Wyngaard, J. C., Izumi, Y. and Bradly, E. F. 1971. Flux profile relationship in the atmospheric surface layer. *J. Atmos. Sci. 28*, 181–189.

Chang, L. W. 1978. Determination of surface flux of

sensible heat, latent heat, and momentum utilizing the bulk Richardson number. *Papers Meteor. Res. 1*, 16–24.

Donner, L. J. 1988. An initialization for cumulus convection in numerical weather prediction models. *Mon. Wea. Rev. 116*, 377–385.

Haltiner, G. J. and Williams, R. T. 1979. *Numerical prediction and dynamic meteorology*. Wiley and Sons. 477 pp.

Harshvardan and Corsetti, T. G. 1984. *Long-wave parameterization for the UCLA/GLAS GCM*. NASA Tech. Mem. 86072, Goddard Space Flight Center, Greenbelt, MD.

Heckley, W. A. 1985. Systematic errors of the ECMWF operational forecasting model in tropical regions. *Quar. Jour. Roy. Met. Soc. 111*, 709–738.

Hoke, J. E. and Anthes, R. A. 1976. The initialization of numerical models by dynamic initialization technique. *Mon. Wea. Rev. 104*, 1551–1556.

Huibang, L. and Yanai, M. 1984. The large-scale circulation and heat sources over the Tibetan Plateau and surrounding areas during the early summer of 1979. Part II: Heat and moisture budgets. *Mon. Wea. Rev. 112*, 966–989.

Johnson, D. R., Yanai, M. and Schaack, T. K. 1987. Global and regional distributions of atmospheric heat sources and sinks during the GWE. *Monsoon meteorology*, Oxford monographs on geology and geophysics, no. 7, pp. 271–297.

Kanamitsu, M. 1975. *On numerical prediction over a global tropical belt*. Report No. 75–1, Available from the Dept. of Meteorology, Florida State University, Tallahassee, Florida 32306, pp. 1–282.

Kanamitsu, N., Tada, K., Kudo, T., Sato, N. and Isa, S. 1983. Description of the JMA operational spectral model. *J. Meteor. Soc. Japan 61*, 812–828.

Kasahara, A., Mizzi, A. P. and Mohanty, U. C. 1987. Comparison of global diabatic heating rates from FGGE level IIIb analyses with satellite radiation imagery data. *Mon. Wea. Rev. 115*, 2904–2935.

Kitade, T. 1983. Nonlinear normal mode initialization with physics. *Mon. Wea. Rev. 111*, 2194–2213.

Krishnamurti, T. N., Cocke, S., Pasch, R. and Low-Nam, S. 1983a. Precipitation estimates from rain gauge and satellite observations summer MONEX, FSU Report No. 83–7, 1–373. Available from Dept. of Meteorology, Florida State University, Tallahassee, Florida 32306.

Krishnamurti, T. N., Low-Nam, S. and Pasch, R. 1983b. Cumulus parameterization and rainfall rates II. *Mon. Wea. Rev. 111*, 815–828.

Krishnamurti, T. N., Ingles, K., Cocke, S., Pasch, R. and Kitade, T. 1984. Details of low latitude medium range numerical weather prediction using a global spectral model II. Effect of orography and physical initialization. *J. Meteor. Soc. Japan 62*, 613–649.

Krishnamurti, T. N. 1986. *Workbook on numerical weather prediction for the tropics for the training of class I and II meteorological personnel*. WMO-No. 669, 335 pp. Available from the World Meteorological Organization.

Krishnamurti, T. N., Low-Nam, S., Kumar, A., Sheng, J. and Sugi, M. 1987. Numerical weather prediction of monsoons. *Monsoon meteorology*. Oxford monographs on geology and geophysics No. 7, pp. 501–544.

Krishnamurti, T. N., Oosterhof, D. K. and Mehta, A. V. 1988a. Air-Sea interaction on the time scale of 30 to 50 days. *J. Atmos. Sci. 45*, 1304–1322.

Krishnamurti, T. N. and Bedi, H. S. 1988b. Cumulus parameterization and rainfall rates: Part III. *Mon. Wea. Rev. 116*, 583–599.

Krishnamurti, T. N., Bedi, H. S., Heckley, W. and Ingles, K. 1988c. Reduction of the spinup time for evaporation and precipitation in a spectral model. *Mon. Wea. Rev. 116*, 907–920.

Krishnamurti, T. N., Bedi, H. S. and Oosterhof, D. K. 1990. Precipitation prediction over the tropics from a global spectral model. *Atmosfera*, 1990, 000–000.

Kuo, H. L. 1965. On formation and intensification of tropical cyclones through latent heat release by cumulus convection. *J. Atmos. Sci. 22*, 40–63.

Kuo, H. L. 1974. Further studies of the parameterization of the influence of cumulus convection on large scale flow. *J. Atmos. Sci. 31*, 1232–1240.

Lacis, A. A. and Hansen, J. E. 1974. A parameterization for the absorption of solar radiation in the earth's atmosphere. *J. Atmos. Sci. 31*, 118–133.

Louis, J. F. 1979. A parametric model of vertical eddy fluxes in the atmosphere. *Bound.-Layer Meteor. 17*, 187–202.

Manobianco, J. 1989. Explosive east coast cyclogenesis: Numerical experimentation and model based diagnostics. *Mon. Wea. Rev. 117*, 2384–2405.

Puri, K. and Miller, M. J. 1990. The use of satellite data in the specification of convective heating for diabatic initialization and moisture adjustment in numerical weather prediction models. *Mon. Wea. Rev. 118*, 67–93.

Stull, R. B. 1988. *An introduction to boundary layer meteorology*. Kluwer Academic Publishers. 666 pp.

Talagrand, O. and Courtier, P. 1987. Variational assimilation of meteorological observation with the adjoint vorticity equation. Part I: Theory. *Quart. J. Roy. Meteor. Soc. 113*, 1311–1328.

Tiedtke, M., Heckley, W. A. and Slingo, J. 1988. Tropical forecasting at ECMWF: On the influence of physical parameterization on the mean structure of forecasts and analyses. *Quart. J. Roy. Meteor. Soc. 114*, 639–664.

Wallace, J. M., Tibaldi, S. and Simmons, A. J. 1983. Reduction of systematic forecast errors in the ECMWF model through the introduction of envelope orography. *Quart. J. Roy. Meteor. Soc. 109*, 683–718.

Yanai, M., Esbensen, S. and Chu, J. H. 1973. Determination of bulk properties of tropical cloud clusters from large-scale heat and moisture budgets. *J. Atmos. Sci. 30*, 611–627.